# Federated Tobit Kalman Filtering Fusion with Dead-Zone-Like Censoring and Dynamical Bias under the Round-Robin Protocol

Hang Geng, Zidong Wang, Fuad E. Alsaadi, Khalid H. Alharbi and Yuhua Cheng

***Abstract*—This paper is concerned with the multi-sensor filtering fusion problem subject to stochastic uncertainties under the Round-Robin protocol (RRP). The uncertainties originate from three sources, namely, censored observations, dynamical biases and additive white noises. To reflect the dead-zone-like censoring phenomenon, the measurement observation is described by the Tobit model where the censored region is constrained by prescribed left- and right-censoring thresholds. The bias is modeled as a dynamical stochastic process driven by a white noise in order to reflect the random behavior of possible ambient disturbances. The RRP is employed to decide the transmission sequence of sensors so as to alleviate undesirable data collisions. The filtering fusion is conducted via two stages: 1) the sensor observations arriving at its corresponding estimator are first leveraged to generate a local estimate, and 2) the local estimates are then gathered together at the fusion center in order to form the fused estimate. The local estimator implements a Tobit Kalman filtering algorithm on the basis of an enhanced Tobit regression model, whilst the fusion center realizes a filtering fusion algorithm in accordance with the well-known federated fusion principle. The validity of the fusion approach is finally shown via a simulation example.**

***Index Terms*—Tobit Kalman filter, censored observations, dynamical bias, federated fusion, Round-Robin protocol.**

## I. Introduction

Multi-sensor data fusion is the process of combining observations from multiple sources to provide a robust and complete description of the interested environment or process [24]. With the rapid advancement of technologies for data sensing, acquisition and analysis, the last few decades have seen an unprecedented prosperity of the multi-sensor data fusion in a great variety of fields including control, filtering, image identification and signal processing. In the context of filtering, the multi-sensor data fusion aims at integrating information from all available sensors in order to reconstruct the interested system state. Accordingly, the multi-sensor data fusion problem is also known as the multi-sensor filtering fusion (MSFF) problem and is, in fact, a state estimation problem based on multiple sensor information. Due to its diverse data sources and strong fault-tolerance, the MSFF is capable of providing better filtering performance as compared with its single sensor counterpart, and has been extensively applied in areas such as fault diagnosis, signal processing, target localization, and sensor networks, see e.g. [16], [24], [46]. Hitherto, a great deal of research effort has been devoted to the investigation on MSFF problems, where the main techniques can be categorized into the centralized filtering fusion and the distributed filtering fusion approaches.

The centralized filtering fusion utilizes a fusion center to gather together all available sensor observations for the purpose of generating the optimal filtering result, whilst the distributed filtering fusion exploits the fusion center to incorporate available estimates from local estimators with a view to producing the optimal/suboptimal filtering result. Owing to its scalable computation overheads, bearable communication costs and strong fault-tolerance capability, the distributed filtering fusion is more favored in engineering practice than its centralized counterpart, where a critical step towards the distributed filtering fusion is the selection of a proper fusion rule from many available ones such as the weighted fusion rule [28], covariance intersection fusion rule [37], federated fusion rule [6], [45], and sequential fusion rule [47], [48].

It has been broadly acknowledged that the MSFF requires not only sensor observations but also mathematical models describing the dynamics of system behavior along with observation models relating sensor outputs to system states. Roughly speaking, the dynamic model is an approximation of the evolution process in relation to the system state that usually cannot be observed directly. In other words, internal disturbance signals and model perturbations are not uncommon in the MSFF, and the resultant dynamical uncertainties would severely restrict the application scope of the MSFF (see [13], [15], [34]). To be more specific, the inherent characteristics of dynamical uncertainties, if inadequately handled, could seriously degrade the system performance, and this has then triggered ever-lasting research enthusiasm towards the analysis and synthesis of uncertainty-corrupted dynamic state estimation, see [26]. Note that most of the forgoing studies have been dedicated to the worst-case scenarios through using

This project was funded by the Deanship of Scientific Research (DSR) at King Abdulaziz University, Jeddah, under grant no. (RG-7-135-41). The authors, therefore, acknowledge with thanks DSR for technical and financial support. This work was also supported in part by the National Natural Science Foundation of China under Grants 61803074, U2030205, 61903065, 61671109, U1830207 and U1830133, the China Postdoctoral Science Foundation under Grants 2017M623005, 2018M643441 and 2015M5825, and the Alexander von Humboldt Foundation of Germany. *(Corresponding author: Yuhua Cheng.)*

H. Geng and Y. Cheng are with the School of Automation Engineering, University of Electronic Science and Technology of China, Chengdu 611731, P. R. China. (Email: yhcheng@uestc.edu.cn)

Z. Wang is with the Department of Computer Science, Brunel University London, Uxbridge, Middlesex, UB8 3PH, United Kingdom. (Email: Zidong.Wang@brunel.ac.uk)

F. E. Alsaadi and K. H. Alharbi are with the Department of Electrical and Computer Engineering, Faculty of Engineering, King Abdulaziz University, Jeddah, 21589, Saudi Arabia.

the upper bound of the uncertainty, which is in addition to an already crude approximation of uncertainty bounds resulting from the often poor prior knowledge. As a result, the final state estimate might be excessively conservative, thereby limits its application scope to a large extent.

Apart from the worst-case investigation, another way of handling the dynamical uncertainty is to carry out the simultaneous state and uncertainty estimation with hope to jointly estimate the state together with the dynamical uncertainty, see e.g. [12], [19], [23]. Stochastic bias, as a specific class of dynamical uncertainty, is often induced by unmodeled dynamics, neglected model nonlinearities, parameter variations and cyber attacks [18], [20], [23]. Stochastic bias is typically described as a dynamical stochastic process (driven by certain white noises) and can be mathematically dealt with by the state augmentation [9], [42] and the dual Kalman filter (KF) approaches [20], [33].

To handle the stochastic bias, the augmentation approach lifts the system state to contain the bias and applies a KF to the resultant system for later state estimation, whilst the dual KF approach employs two KFs to estimate the state and bias simultaneously and update each other's estimates mutually. Very recently, the joint estimation problem of state and dynamical bias has been investigated in [42] for two-dimensional systems with shift-varying parameters, where the augmentation technique has been adopted to tackle the stochastic bias and the prescribed filtering performance has been ensured by minimizing the upper bound of the acquired error covariance in the sense of matrix-trace.

Due to the utilization of massive low-cost commercial off-the-shelf sensors, the MSFF might be prone to a peculiar sort of measurement nonlinearity, i.e. censored observations, see [5], [14]. Censored/saturated observations result primarily from intrinsic physical constraints (on system dynamics) and/or disturbances from neighboring systems. The phenomenon of censored observations, if inadequately handled, are likely to impair the system performance, causing undesirable oscillation or even leading to instability [3], [6]. Mathematically, the censored observation can be described as a piecewise-linear transformation of the output variable with a zero slope in the censored region. Based on this description, the relevant filtering problem has been a subject of extensive investigation by using fairly mature estimation techniques. Among various filters proposed so far, we highlight the iterative KF [38], particle filter [49] and Tobit Kalman filter (TKF) [1], [2] that have proven to be rather popular.

In the context of censoring-oriented filtering, the so-called TKF stands out as a competitive approach with practical significance. A remarkable feature of the TKF is that, at a moderate computational burden, it offers a completely recursive estimation paradigm identical to the standard KF [1].Since its initialization, the TKF problem has stirred much research enthusiasm and a number of excellent results have been acquired with successful applications in a great variety of fields such as target tracking [26], unmanned aerial vehicle positioning [11] and fault detection problems [22]. More recently, a distributed TKF has been devised in [14] under the federated fusion rule with its performance assessed from a probabilistic viewpoint. It is worth pointing out that most aforementioned literature has been concerned with the setting of one-side censoring, whereas the two-side censoring (i.e. the dead-zone-like censoring) setting has been largely overlooked despite its pervasive existence in a great variety of physical reality suffering from sensor saturations, detection limitations, and image frame effects, see e.g. [2], [22], [41].

In the past few decades, the networked systems have become more and more popular as a response to the increasing demands from engineering practice including communication, patient monitoring and target localization [8], [21], [25], [28], [29], [48], [51], [52]. In an ideal situation, *all* system components (e.g. actuators, controllers, filters and sensors) have equal privileges for information propagation via shared medium. This supposition is, however, often impractical as limited-bandwidth-induced data collisions are likely to happen when information exchanges take place simultaneously by more than one component. To handle the network-induced challenges, an effective measure is to leverage communication protocols so as to regulate the data transmission, and some widely deployed protocols include the Round-Robin protocol (RRP), try-once-discard protocol, and random access protocols protocol (see e.g. [37], [39], [40], [50]), where the RRP is particularly welcomed in industry because of its succinct execution in allocating network resources. Under the RRP, the information propagation among system components is implemented in a *fixed circular* order [7], [53]. Nevertheless, very few results have been acquired so far on the protocol-based Tobit Kalman filtering fusion problem, not to mention the case where the dynamical biases and the dead-zone-like censoring are both involved.

Following the discussions made thus far, we conclude that there is a lack of systematic investigation on bias-corrupted multi-sensor Tobit Kalman filtering fusion problems subject to dead-zone-like censoring under the RRP. As such, the primary objective of this paper is to fill in such a gap by designing a protocol-based federated Tobit Kalman filter (FTKF) that is insensitive to dynamical biases and censored observations. This topic, though theoretically important and practically significant, is quite challenging for three reasons given below.

- For the dynamical bias, its correlation with the state as well as the sensor observations renders substantial complexities to the analysis of the multi-sensor model, and it remains challenging to resolve such a correlation.
- For the RRP, the transmission of the sensor information is executed in a *fixed circular* sequence and, consequently, dedicated effort needs to be made on the establishment of a modified Tobit regression model that accommodates such a fixed circular sequence along with the dynamical bias.
- In view of the concurrence of dead-zone-like censoring, dynamical bias and RRP, their impacts on the performance of the desired filter should be examined in a rigorous way.

In response to the identified challenges, the primary contributions we deliver in this paper are outlined in threefold as

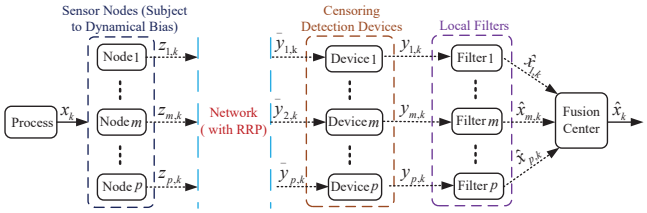


Fig. 1: Schematic diagram for the concerned Tobit Kalman filtering problem.

follows.

- To our knowledge, one of the first few attempts is made in this paper to look into the Tobit Kalman filtering fusion problems with the dead-zone-like censoring and RRP fashion under the federated fusion rule, where the system model is both holistic and comprehensive in catering for general practices.
- Compared with the conventional TKF in [2], our newly devised filter produces both state and bias estimates in the multi-sensor scenario with the help of the augmentation technique, and a suite of new terms (including the augmented state, the product of the measurement update matrix and augmented state together with the associate error covariances) arise, which is seen as an envisioned reflection of the addressed dead-zone-like censoring, dynamical biases and RRP.
- The proposed algorithm is of a recursive manner and is therefore favorable for online applications.

The rest of this paper is highlighted as follows. In Section II, the problem under consideration is formulated. In Section III, an ameliorated Tobit regression model is built, based on which a protocol-based FTKF is designed. In Section IV, a numerical example is provided to show the usefulness of the filter, and some conclusions are drawn in Section V.

**Notation** The notation used here is fairly standard except where otherwise stated. $\mathbb{R}^n$ denotes the *n*-dimensional Euclidean space. "$I$"and "0" respectively, represent identity and zero matrices with compatible dimensions. Superscripts "-1" and "$T$" represent inverse and transpose operations, respectively. $\mathbb{E}\{x\}$ and $\mathbb{E}\{x|y\}$ will, respectively, mean the expectation of $x$ and the expectation of $x$ conditional on $y$. diag$\{X_m\}$ $(m=1,2,\ldots,p)$ stands for a block-diagonal matrix with matrices $X_m$ on the diagonal. vec$\{x_m\} \triangleq \begin{bmatrix} x_1 & x_2 & \cdots & x_p \end{bmatrix}^T$. var$\{x\}$ denotes the variance of $x$. $\delta(\cdot) \in \{0,1\}$ is the Dirac delta function.

## II. Problem Formulation

Consider the Tobit Kalman filtering problem for a networked system as shown in Fig. 1. In this framework, the sensor is susceptible to dynamical biases, the signal transmission between the sensor and the local filter is implemented through a communication network under the RRP, and the measurement arriving at the filter is inclined to dead-zone-like censoring. State estimates collected from local filters are later sent to the fusion center for further process so as to achieve the integrated filtering result. In what follows, let us introduce the plant, dynamical bias, communication network, and dead-zone-like censoring in a mathematical way.

Consider a multi-sensor system corrupted by dynamical biases [20], [42]:

$$x_{k+1} = A_k x_k + B_k b_k + \omega_k, \tag{1}$$
$$z_{m,k} = C_{m,k} x_k + \upsilon_{m,k}, m = 1,2,\ldots,p, \tag{2}$$

where $x_k \in \mathbb{R}^{n_x}$ is the state vector, $z_{m,k} \in \mathbb{R}$ is the uncensored observation of the $m$th $(m=1,2,\ldots,p)$ sensor and $p$ is the total number of sensors. $A_k$, $B_k$ and $C_{m,k}$ are known matrices with eligible dimensions. $\omega_k \in \mathbb{R}^{n_x}$ and $\upsilon_{m,k} \in \mathbb{R}$ are zero-mean white Gaussian noises with covariances $Q_k$ and $R_{m,k}$, respectively. Here, $b_k \in \mathbb{R}^{n_b}$ is the stochastic bias driven by the following dynamic equation:

$$b_k = H_{k-1} b_{k-1} + \varepsilon_{k-1}, \tag{3}$$

where $H_k$ is the known bias transition matrix, and $\varepsilon_k$ is the white Gaussian noise with zero mean and covariance $\Xi_k$.

In maneuvering target tracking, the target manoeuver is usually modeled as an unknown acceleration bias to the constant velocity model as shown in (1), where $x_k$ consists of the target position and velocity and $b_k$ is the acceleration bias [44]. By closely observing the target manoeuver, one is capable of deciding whether the dynamics of the unknown acceleration bias given by (3) should be characterized by a constant acceleration model or a variable acceleration model. In the event that (3) is a constant acceleration model, one certainly has $H_k = I$ for all $k \geq 1$. This example explicitly tells us that, the bias transition matrix $H_k$ can be determined beforehand according to the concerned engineering scenario. As such, $H_k$ is assumed to be known a priori in this paper.

Note that the observations $z_{m,k} \in \mathbb{R}$ $(m=1,2,\ldots,p)$ are transmitted to the remote estimator via a shared communication network. Due to limited communication bandwidth, the communication protocol is often deployed with which only one single sensor is granted to propagate its output, at each communication time, through the shared network. As discussed in the introduction, in this paper, the RRP is employed to orchestrate the transmission order of the sensors for the purpose of circumventing data collisions.

Denote mod$(k-m,p)$ as the unique non-negative remainder on division of $k-m$ by $p$, and $\hbar_k \in \{1,2,\ldots,p\}$ as the sensor that has access to the network at time $k$. Let

$$\Gamma_{\hbar_k} \triangleq \text{diag}\{\Gamma_{m,\hbar_k}\}, \quad m=1,2,\ldots,p$$

be the observation update coefficient where

$$\Gamma_{m,\hbar_k} \triangleq \delta(\hbar_k - m).$$

Abiding by the RRP and the zero-order holder strategy, for the $m$th sensor, the actual measurement $\bar{y}_{m,k}$ arriving at the remote estimator after network transmission is updated as follows (see [53]):

$$\bar{y}_{m,k} = \begin{cases} z_{m,k}, & \text{if mod}(k-m,p)=0, \\ \bar{y}_{m,k-1}, & \text{otherwise.} \end{cases} \tag{4}$$

Taking advantage of the update coefficient $\Gamma_{\hbar_k}$, (4) can be rearranged into

$$\bar{y}_{m,k} = \sum_{l=0}^{p-1} \Gamma_{m,\hbar_{k-l}} z_{m,k-l}, \tag{5}$$

where $\hbar_{k-l} \triangleq l$ and $z_{m,k-l} \triangleq z_{m,0}$ for $k-l \leq 0$.

Let the input terminal of the remote estimator be equipped with an additional detection device whose function is to check whether $\bar{y}_{m,k}$ is censored or not. In this sense, the Tobit observation model with dead-zone-like censoring is given as follows (see [2]):

$$y_{m,k} = \begin{cases} \tau_m^l, & \bar{y}_{m,k} \leq \tau_m^l, \\ \bar{y}_{m,k}, & \tau_m^l < \bar{y}_{m,k} < \tau_m^r, \\ \tau_m^r, & \bar{y}_{m,k} \geq \tau_m^r, \end{cases} \tag{6}$$

where $y_{m,k}$ is the censored observation, and $\tau_m^l$ and $\tau_m^r$ are, respectively, the left- and right-censoring thresholds.

According to whether $\bar{y}_{m,k}$ is left-censored, right-censored or uncensored, the observation model (6) is rewritten as

$$y_{m,k} = (1-\alpha_{m,k}-\beta_{m,k})\bar{y}_{m,k} + \alpha_{m,k}\tau_m^l + \beta_{m,k}\tau_m^r, \tag{7}$$

where $\alpha_{m,k}$ and $\beta_{m,k}$ are, respectively, Bernoulli random variables governing the left- and right-censoring phenomena of $\bar{y}_{m,k}$ with following probability distributions:

$$\begin{cases} \text{Prob}\{\alpha_{m,k}=1\} = \bar{\alpha}_{m,k}, \\ \text{Prob}\{\beta_{m,k}=1\} = \bar{\beta}_{m,k}, \\ \text{Prob}\{\alpha_{m,k}=0\} = 1-\bar{\alpha}_{m,k}, \\ \text{Prob}\{\beta_{m,k}=0\} = 1-\bar{\beta}_{m,k}. \end{cases} \tag{8}$$

Here, $\bar{\alpha}_{m,k}$ and $\bar{\beta}_{m,k}$ are non-negative constants that are known *a priori*, and $\alpha_{m,k}$ and $\beta_{m,k}$ are uncorrelated with $\omega_k$ and $\varepsilon_k$.

Let

$$\begin{aligned} y_{m,1:k} &\triangleq \{y_{m,0}, y_{m,1}, \ldots, y_{m,k}\}, \\ \hat{x}_{m,k}^- &\triangleq \mathbb{E}\{x_k | y_{m,1:k-1}\}, \\ \hat{y}_{m,k}^- &\triangleq \mathbb{E}\{y_{m,k} | y_{m,1:k-1}\}, \\ \hat{x}_{m,k} &\triangleq \mathbb{E}\{x_k | y_{m,1:k}\}, \\ \tilde{x}_{m,k}^- &\triangleq x_k - \hat{x}_{m,k}^-, \\ \tilde{x}_{m,k} &\triangleq x_k - \hat{x}_{m,k}, \\ P_{\tilde{x}_{m,k}} &\triangleq \mathbb{E}\{\tilde{x}_{m,k}\tilde{x}_{m,k}^T\}, \\ P_{\tilde{x}_{m,k}^-} &\triangleq \mathbb{E}\left\{\tilde{x}_{m,k}^- \left(\tilde{x}_{m,k}^-\right)^T\right\}. \end{aligned}$$

*Assumption 1:* 1) The initial state $x_0$ and the bias $b_0$ have means $\bar{x}_0$ and $\bar{b}_0$, and covariances $P_{\tilde{x}_0}$ and $P_{\tilde{b}_0}$, respectively. 2) The random variables $x_0$, $b_0$, $\omega_k$, $\varepsilon_k$ and $\upsilon_{m,k}$ are mutually independent.

*Remark 1:* In system modeling, ambient disturbances provoked by environmental variations are often regarded as process noises taking the form of Gaussian white sequences. Such a treatment ignores the case where the disturbance might exhibit itself as a dynamically varying process, namely, the stochastic bias. As a matter of fact, stochastic biases (stemming from random frictions, wind resistance and/or electromagnetic interferences) might behave according to a dynamical manner similar to the evolution of the target system. Spurred by this fact, the random variable $b_k$ is introduced in this paper to characterize the stochastic bias with its evolution kinetics being governed by (3).

*Remark 2:* Under the scheduling of the RRP, equal priority is assigned to each sensor and the observation from individual sensor is admitted to enter the network in a *fixed circular* manner. In comparison with other communication protocols (e.g. the try-once-discard protocol and random access protocol), the RRP predefines a periodic transmission rule which makes the scheduling easy-to-implement. Therefore, the RRP is adopted in this paper as the desired communication protocol for data transmission.

In the case that sensor $m$ has no access to the network, two strategies (i.e. the zero-input and zero-order holder strategies) are often leveraged to establish the actual observation $\bar{y}_{m,k}$ that is received by the remote estimator. As suggested by their names, the null and previous measurements are, respectively, employed as compensatory inputs to the remote estimator in the two strategies in case of transmission failures. The selection between the two strategies rides on the actual network condition and the performance requirements. Here, the zero-order holder strategy is utilized to generate $\bar{y}_{m,k}$ for the purpose of offsetting $\bar{y}_{m,k}$. Accordingly, at time $k-l$, only the observation $\bar{y}_{\hbar_{k-l},k-l}$ is adopted for later filter update, whilst the rest sensor observations $\bar{y}_{m,k-l}$ $(m=1,2,\ldots,p,$ $m \neq \hbar_{k-l})$ remain the same as their counterparts in $\bar{y}_{k-l-1}$. Obeying the *fixed circular* order for information propagation, $\bar{y}_{m,k}$ $(m=1,2,\ldots,p)$ can be represented by the sum of $\Gamma_{m,\hbar_{k-l}} z_{m,k-l}$ $(l=0,1,\ldots,p-1)$ as shown in (5).

In practice there exist two typical communication channels in multi-sensor fusion application scenarios, i.e. the sensor-to-estimator and estimator-to-fusion-center communication channels. Frankly speaking, the sensor-to-estimator channel is long as the estimator is normally located far away from the sensor in order to obtain a reliable environment for the implementation of the estimation algorithm, whilst the estimator-to-fusion-center channel is short as local estimators are placed close to the fusion center to guarantee that local estimates are perfectly transmitted for final fusion. Accordingly, the sensor-to-estimator channel is easily susceptible to noises and disturbances, while the estimator-to-fusion-center channel normally appears to be noise-free and perfect. In this regard, comparing with the estimator-to-fusion-center channel , the sensor-to-estimator channel is more likely to be subject to bandwidth limitations. As such, the Round-Robin protocol is implemented in the sensor-to-estimator channel with a view point to regulating the data transmission and mitigating the data collision.

*Remark 3:* The dead-zone-like censoring modeled by (6) is widely encountered in systems equipped with low-cost commercial off-the-shelf sensors. The distinctive feature of such censoring lies in its censored Gaussian (rather than pure Gaussian) noise distribution at/near the censored region, and this circumvents the direct employment of the conventional KF. The necessity of formulating a censoring-oriented KF

gives birth to the celebrated TKF. By bringing in Bernoulli random variables to regulate the censoring phenomenon, the TKF perfectly handles the non-Gaussianity of the observation noise via developing a so-called Tobit regression model, based at which an explicit paradigm of the observation expectation and variance is provided. When the target plant is prone to dynamical biases, the standard TKF fails to take effect accounting for the bias-induced variations that enter into the system dynamics, the regression model as well as the filter equations. Moreover, the adoption of the RRP would ineluctably pose significant impacts on the structure of the regression model, censoring probability together with other observation related terms. As such, a holistic multi-sensor Tobit Kalman filtering fusion framework is constructed in this article to solve the aforementioned problems.

It is observed from (7) that, random variables $\alpha_{m,k}$ and $\beta_{m,k}$ are exploited to describe the censoring phenomena of $\bar{y}_{m,k}$. In accordance with (7), if no censoring occurs for $\bar{y}_{m,k}$, i.e. $\alpha_{m,k} = 0$ and $\beta_{m,k} = 0$, the measurement becomes $y_{m,k} = \bar{y}_{m,k}$, which means that the observation is equivalent to the latent one. If the left-censoring occurs for $\bar{y}_{m,k}$, i.e. $\alpha_{m,k} = 1$ and $\beta_{m,k} = 0$, the measurement becomes $y_{m,k} = \tau_m^l$, which means that the left-censoring threshold is allocated to the observation. If the right-censoring occurs for $\bar{y}_{m,k}$, i.e. $\alpha_{m,k} = 0$ and $\beta_{m,k} = 1$, the measurement becomes $y_{m,k} = \tau_m^r$, which means that the right-censoring threshold is allocated to the observation. Here, we suppose that censoring probabilities $\bar{\alpha}_{m,k}$ and $\bar{\beta}_{m,k}$ are known *a priori* via some statistical experiments. Alternatively, drawing inspiration from [1], [2], $\bar{\alpha}_{m,k}$ and $\bar{\beta}_{m,k}$ can also be approximated by

$$\begin{cases} \bar{\alpha}_{m,k} \approx \Phi\left(\dfrac{\tau_m^l - \hat{\zeta}_{m,k}^-}{\sqrt{\mathcal{R}_{m,k}}}\right), \\ \bar{\beta}_{m,k} \approx \Phi\left(\dfrac{\hat{\zeta}_{m,k}^- - \tau_m^r}{\sqrt{\mathcal{R}_{m,k}}}\right), \end{cases} \tag{9}$$

where

$$\mathcal{R}_{m,k} \triangleq \sum_{l=0}^{p-1} \Gamma_{m,\hbar_{k-l}}^2 R_{m,k-l},$$

$$\hat{\zeta}_{m,k}^- \triangleq \Gamma_{m,\hbar_k} C_{m,k} \hat{x}_k^- + \sum_{l=1}^{p-1} \Gamma_{m,\hbar_{k-l}} C_{m,k-l} \hat{x}_{k-l},$$

and $\Phi(\cdot)$ is the cumulative distribution function (CDF) of the random variable "$\cdot$" that obeys the standard normal distribution.

The objectives of this paper is to design a protocol-based FTKF for system (1)–(8) subject to dead-zone-like censoring and dynamical biases under the RRP.

## III. The Main Results

In this section, we are devoted to formalize a federated Tobit Kalman filtering fusion framework to overcome the identified multi-faceted challenges caused by the concurrence of dead-zone-like censoring, dynamical bias and RRP. Such a framework displays its distinctive characters from two viewpoints: 1) an elaborately designed local Tobit Kalman filters (LTKFs) built on an enhanced regression model that gives holistic consideration of the impacts incurred by the dead-zone-like censoring, dynamical bias and RRP, where additional endeavor is demanded to compute the observation prediction, filter gain as well as associate error covariances; 2) elegantly opted fusion rule which productively integrates available estimates from LTKFs, where the global optimality of the fused estimate is ensured.

Denoting

$$\xi_k \triangleq \begin{bmatrix} x_k^T & b_k^T \end{bmatrix}^T,$$
$$w_k \triangleq \begin{bmatrix} \omega_k^T & \varepsilon_k^T \end{bmatrix}^T,$$

system (1)–(8) is augmented as

$$\xi_{k+1} = \mathcal{A}_k \xi_k + \mathcal{B}_k w_k, \tag{10}$$
$$z_{m,k} = \mathcal{C}_{m,k} \xi_k + \upsilon_{m,k}, \tag{11}$$

where

$$\mathcal{A}_k = \begin{bmatrix} A_k & B_k \\ 0 & H_k \end{bmatrix}, \mathcal{B}_k = \begin{bmatrix} I & 0 \\ 0 & I \end{bmatrix}, \mathcal{C}_{m,k} = \begin{bmatrix} C_{m,k} & 0 \end{bmatrix}.$$

Let

$$\begin{aligned} \bar{y}_{m,k} &\triangleq \zeta_{m,k} + \nu_{m,k}, \\ \zeta_{m,k} &\triangleq \sum_{l=0}^{p-1} \Gamma_{m,\hbar_{k-l}} C_{m,k-l} \xi_{k-l}, \\ \nu_{m,k} &\triangleq \sum_{l=0}^{p-1} \Gamma_{m,\hbar_{k-l}} \upsilon_{m,k-l}, \\ \vartheta_{m,k}^l &\triangleq \frac{\tau_m^l - \zeta_{m,k}}{\mathcal{R}_{m,k}}, \\ \vartheta_{m,k}^r &\triangleq \frac{\tau_m^r - \zeta_{m,k}}{\mathcal{R}_{m,k}}. \end{aligned}$$

On the basis of the augmented model (10)–(11), an enhanced Tobit regression is formulated as follows to accommodate the dead-zone-like censoring, dynamical bias and RRP influences.

*Lemma 1:* The expectation and variance of $y_{m,k}$ $(m = 1, 2, \ldots, p)$ are, respectively,

$$\begin{aligned} \mathbb{E}\left\{y_{m,k} | x_k, \mathcal{R}_{m,k}\right\} =& \Phi\left(\vartheta_{m,k}^l\right) \tau_m^l + \left(1 - \Phi\left(\vartheta_{m,k}^r\right)\right) \tau_m^r \\ &+ \left[\Phi\left(\vartheta_{m,k}^r\right) - \Phi\left(\vartheta_{m,k}^l\right)\right] \\ &\times \left[\zeta_{m,k} - \sqrt{\mathcal{R}_{m,k}} \lambda\left(\vartheta_{m,k}^r, \vartheta_{m,k}^l\right)\right], \end{aligned} \tag{12}$$

$$\operatorname{var}\left\{y_{m,k} | x_k, \mathcal{R}_{m,k}\right\} = \mathcal{R}_{m,k}\left[1 + \varphi\left(\vartheta_{m,k}^r, \vartheta_{m,k}^l\right)\right], \tag{13}$$

where

$$\lambda\left(\vartheta_{m,k}^r, \vartheta_{m,k}^l\right) = \frac{\phi\left(\vartheta_{m,k}^r\right) - \phi\left(\vartheta_{m,k}^l\right)}{\Phi\left(\vartheta_{m,k}^r\right) - \Phi\left(\vartheta_{m,k}^l\right)}, \tag{14}$$

$$\begin{aligned} \varphi\left(\vartheta_{m,k}^r, \vartheta_{m,k}^l\right) =& \frac{\vartheta_{m,k}^l \phi\left(\vartheta_{m,k}^l\right) - \vartheta_{m,k}^r \phi\left(\vartheta_{m,k}^r\right)}{\Phi\left(\vartheta_{m,k}^r\right) - \Phi\left(\vartheta_{m,k}^l\right)} \\ &- \lambda^2\left(\vartheta_{m,k}^r, \vartheta_{m,k}^l\right). \end{aligned} \tag{15}$$

Here, $\phi(\cdot)$ and $\Phi(\cdot)$ are, respectively, the probability density function (PDF) and CDF of the Gaussian random variable $\vartheta_{m,k} \in \{\vartheta^r_{m,k}, \vartheta^l_{m,k}\}$ with following forms:

$$\phi(\vartheta_{m,k}) = \frac{1}{\sqrt{2\pi}} e^{-\frac{\left(\tau_m - \zeta_{m,k}\right)^2}{2\mathcal{R}_{m,k}}}, \tag{16}$$

$$\Phi(\vartheta_{m,k}) = \int_{-\infty}^{\tau_m} \frac{1}{\sqrt{2\pi\mathcal{R}_{m,k}}} e^{-\frac{\left(y_{m,k} - \zeta_{m,k}\right)^2}{2\mathcal{R}_{m,k}}} d_{y_{m,k}}, \tag{17}$$

where $\tau_m \in \{\tau^r_m, \tau^l_m\}$.

*Proof:* See Appendix–A. ∎

*Remark 4:* The enhanced regression model in Lemma 1 explicitly supplies us with the specific expressions of the observation mean and variance in case of dead-zone-like censoring, dynamical bias and RRP. In contrast with its single sensor counterpart in [2], it is evidently seen that, a suite of terms ($\mathbb{E}\{y_{m,k}|x_k, \mathcal{R}_{m,k}\}$ and $\text{var}\{y_{m,k}|x_k, \mathcal{R}_{m,k}\}$) appear here that carry the multi-sensor information. In addition, due to the concurrence of the RRP and dynamical bias, the term $C_k x_k$ is substituted by an augmented and delayed state $\zeta_{m,k} \triangleq \sum_{l=0}^{p-1} \Gamma_{m,\hbar_{k-l}} C_{m,k-l} \xi_{k-l}$, and the noise covariance $R_{m,k}$ is replaced by an equivalent covariance $\mathcal{R}_{m,k} \triangleq \sum_{l=0}^{p-1} \Gamma^2_{m,\hbar_{k-l}} R_{m,k-l}$. Note that the presence of these new terms will inevitably result in 1) the development of a bank of LTKFs; 2) the substitution of $C_k x_k$ and $R_{m,k}$, respectively, by $\zeta_{m,k}$ and $\mathcal{R}_{m,k}$ throughout all observation related terms; and 3) the emergence of several new terms in regard to $\zeta_{m,k}$ and $\mathcal{R}_{m,k}$ that further sophisticates the later filter design.

Let

$$\begin{aligned}
\hat{\xi}^-_{m,k} \triangleq& \mathbb{E}\{x_k|y_{m,1:k-1}\},\\
\hat{\xi}_{m,k} \triangleq& \mathbb{E}\{\xi_k|y_{m,1:k}\},\\
\tilde{\xi}^-_{m,k} \triangleq& \xi_k - \hat{\xi}^-_{m,k},\\
\hat{y}^-_{m,k} \triangleq& \mathbb{E}\{y_{m,k}|y_{m,1:k-1}\},\\
\tilde{y}^-_{m,k} \triangleq& y_{m,k} - \hat{y}^-_{m,k},\\
\tilde{\xi}_{m,k} \triangleq& \xi_k - \hat{\xi}_{m,k},\\
P_{\tilde{\xi}^-_{m,k}} \triangleq& \mathbb{E}\{\tilde{\xi}^-_{m,k}(\tilde{\xi}^-_{m,k})^T\},\\
P_{\tilde{\xi}_{m,k}} \triangleq& \mathbb{E}\{\tilde{\xi}_{m,k}\tilde{\xi}^T_{m,k}\},\\
P_{\tilde{\xi}^-_{m,k}\tilde{y}^-_{m,k}} \triangleq& \mathbb{E}\{\tilde{\xi}^-_{m,k}(\tilde{y}^-_{m,k})^T\},\\
\bar{\vartheta}^l_{m,k} \triangleq& \frac{\tau^l_m - \hat{\zeta}^-_{m,k}}{\mathcal{R}_{m,k}},\\
\bar{\vartheta}^r_{m,k} \triangleq& \frac{\tau^r_m - \hat{\zeta}^-_{m,k}}{\mathcal{R}_{m,k}},\\
\hat{\zeta}^-_{m,k} \triangleq& \sum_{l=1}^{p-1} \Gamma_{m,\hbar_{k-l}} \mathcal{C}_{m,k-l} \hat{\xi}_{k-l} + \Gamma_{m,\hbar_k} \mathcal{C}_{m,k} \hat{\xi}^-_k.
\end{aligned}$$

Before proceeding further, we first introduce the following federated information distribution and fusion principle.

*Lemma 2:* [6] Suppose that $\hat{x}_{m,k}$ $(m = 1, 2, \ldots, p)$ and $P_{m.k}$ are, respectively, the estimate and covariance of a stochastic $n_x$-dimension vector $x_k$ obtained by the $m$th local estimator, $\hat{x}_k$ and $P_k$ are, respectively, the global optimal estimate and covariance obtained by the fusion estimator under the federated Kalman fusion rule, and $Q_k$ is the covariance of the process noise. Then, the information sharing process among the local estimators and the fusion estimator is as follows:

$$\begin{cases} Q_{i,k-1} = \epsilon_m^{-1} Q_{k-1}, \\ P_{m,k-1} = \epsilon_m^{-1} P^f_{k-1}, \\ \hat{x}_{m,k-1} = \hat{x}_{k-1}, \end{cases}$$

where $\epsilon_m$ are the information sharing coefficients satisfying $\sum_{m=1}^{p} \epsilon_m = 1$. Moreover, the fused estimate and covariance of $x_k$ are given as

$$\begin{cases} P_k = \left( \sum_{m=1}^{p} P^{-1}_{m,k} \right)^{-1}, \\ \hat{x}_k = P_k \left( \sum_{m=1}^{p} P^{-1}_{m,k} \hat{x}_{m,k} \right). \end{cases}$$

In line with Lemmas 1–2, the customized LTKF (susceptible to dead-zone-like censoring, dynamical bias and RRP) is presented as follows.

*Theorem 1:* The LTKF for system (10)–(11) is of the following structure:

$$\hat{\xi}^-_{m,k} = \mathcal{A}_{k-1} \hat{\xi}_{m,k-1}, \tag{18}$$

$$P_{\tilde{\xi}^-_{m,k}} = \mathcal{A}_{k-1} P^T_{\tilde{\xi}_{m,k-1}} \mathcal{A}^T_{k-1} + \mathcal{B}_{k-1} Q_{m,k-1} \mathcal{B}^T_{k-1}, \tag{19}$$

$$\hat{\xi}_{m,k} = \hat{\xi}^-_{m,k} + K_{m,k}(y_{m,k} - \hat{y}^-_{m,k}), \tag{20}$$

$$P_{\tilde{\xi}_{m,k}} = P_{\tilde{\xi}^-_{m,k}} - K_{m,k} P^T_{\tilde{\xi}^-_{m,k}\tilde{y}^-_{m,k}}. \tag{21}$$

The local filtering gain matrix $K_{m,k}$ and one-step measurement prediction are

$$K_{m,k} = P_{\tilde{\xi}^-_{m,k}\tilde{y}^-_{m,k}} P^{-1}_{\tilde{y}^-_{m,k}}, \tag{22}$$

$$\begin{aligned}
\hat{y}^-_{m,k} =& \bar{\alpha}_{m,k} \tau^l_m + \bar{\beta}_{m,k} \tau^r_m + (1 - \bar{\alpha}_{m,k} - \bar{\beta}_{m,k}) \\
&\times \left[ \hat{\zeta}^-_{m,k} + \sqrt{\mathcal{R}_{m,k}} \lambda \left( \bar{\vartheta}^r_{m,k} - \bar{\vartheta}^l_{m,k} \right) \right],
\end{aligned} \tag{23}$$

where

$$\begin{aligned}
&P_{\tilde{\xi}^-_{m,k}\tilde{y}^-_{m,k}} \\
=& (1 - \bar{\alpha}_{m,k} - \bar{\beta}_{m,k}) P_{\tilde{\xi}^-_k} \left( \Gamma_{m,\hbar_k} C_{m,k} \right)^T,
\end{aligned} \tag{24}$$

$$\begin{aligned}
&P_{\tilde{y}^-_{m,k}} \\
=& (1 - \bar{\alpha}_{m,k} - \bar{\beta}_{m,k})^2 \Gamma_{m,\hbar_k} C_{m,k} P_{\tilde{\xi}^-_k} C^T_{m,k} \Gamma_{m,\hbar_k} \\
&+ (1 - \bar{\alpha}_{m,k} - \bar{\beta}_{m,k})^2 \sum_{l=1}^{p-1} \Gamma_{m,\hbar_{k-l}} C_{m,k-l} P_{\tilde{\xi}_{k-l}} \\
&\times C^T_{m,k-l} \Gamma_{m,\hbar_{k-l}} + \mathcal{R}_{m,k} \left[ 1 + \varphi\left( \bar{\vartheta}^r_{m,k}, \bar{\vartheta}^l_{m,k} \right) \right].
\end{aligned} \tag{25}$$

*Proof:* See Appendix–B. ∎

*Remark 5:* When making comparison between the proposed LTKF in Theorem 1 and the conventional TKF in [2], we observe three major differences. The first difference is the replacement of the $C_k \hat{x}^-_k$ (which is the product of the original observation coefficient $C_k$ and state prediction $\hat{x}^-_k$) by $\hat{\zeta}^-_{m,k} \triangleq \sum_{l=0}^{p-1} \Gamma_{m,\hbar_{k-l}} C_{m,k-l} \hat{\xi}^-_{k-l}$ (which is the sum of $p$ products in regard to the update coefficient $\Gamma_{m,\hbar_{k-l}}$, observation coefficient $C_{m,k-l}$ and augmented state $\xi_{k-l}$)

in all observation related terms. The second difference is the substitution of the original observation noise covariance $R_{m,k}$ by $\mathcal{R}_{m,k} \triangleq \sum_{l=0}^{p-1} \Gamma^2_{m,\hbar_{k-l}} R_{m,k-l}$ (which is the sum of $p$ delayed noise covariances) in all terms relevant to the observation prediction, filter gain as well as error covariances. The last difference is the presence of several new terms including the augmentation-induced terms $\hat{\xi}^-_{m,k}$, $\hat{\xi}_{m,k}$, $P_{\tilde{\xi}^-_{m,k}}$, $P_{\tilde{\xi}_{m,k}}$, $P_{\tilde{\xi}^-_{m,k}\tilde{y}^-_{m,k}}$ and the protocol-induced terms $\bar{\gamma}_{m,k}\sum_{l=1}^{p-1} C_{m,k-l} P_{\tilde{\xi}_{m,k-l}} \mathcal{C}^T_{m,k-l}\bar{\gamma}_{m,k}$. These differences obviously reflect the influences from the dynamical bias and the RRP on the development of the filtering fusion algorithm.

*Theorem 2:* Suppose that $\hat{\xi}_{m,k}$ $(m = 1, 2, \ldots, p)$ and $P_{\tilde{\xi}_{m,k}}$ are, respectively, the state estimate and the error covariance produced by the $m$th LTKF. Let $\hat{\xi}_k$ and $P_{\tilde{\xi}_k}$ be, respectively, the global optimal estimate and covariance obtained at the fusion center under the federated fusion rule. Then, the FTKF for system (10)–(11) is expressed as

$$\begin{cases} P_{\tilde{\xi}_k} = \left( \sum_{m=1}^{p} P^{-1}_{\tilde{\xi}_{m,k}} \right)^{-1}, \\ \hat{\xi}_k = P_{\tilde{\xi}_k} \left( \sum_{i=1}^{p} P^{-1}_{\tilde{\xi}_{m,k}} \hat{\xi}_{m,k} \right). \end{cases} \tag{26}$$

where

$$\begin{cases} Q_{m,k-1} = \epsilon_m^{-1} Q_{k-1}, \\ P_{\tilde{\xi}_{m,k-1}} = \epsilon_m^{-1} P_{\tilde{\xi}_{k-1}}, \\ \hat{\xi}_{m,k-1} = \hat{\xi}_{k-1}. \end{cases} \tag{27}$$

Denoting

$$\Gamma_1 \triangleq \begin{bmatrix} I & 0 \end{bmatrix}, \\ \Gamma_2 \triangleq \begin{bmatrix} 0 & I \end{bmatrix},$$

the next theorem presents the FTKF for system (1)–(8).

*Theorem 3:* Given system (1)–(8), its FTKF is as follows:

$$\begin{cases} \hat{x}_k = \Gamma_1 \hat{\xi}_k, \\ \hat{b}_k = \Gamma_2 \hat{\xi}_k, \\ P_{\tilde{x}_k} = \Gamma_1 P_{\tilde{\xi}_k} \Gamma_1^T, \\ P_{\tilde{b}_k} = \Gamma_2 P_{\tilde{\xi}_k} \Gamma_2^T. \end{cases} \tag{28}$$

*Proof:* Theorem 3 follows readily from Theorem 1 by noting the correlation between system (1)–(8) and system (10)–(11). ■

Theorems 1–2, together with Lemma 1, constitute the FTKF algorithm with its pseudocode outlined in Table I.

*Remark 6:* In accordance with Lemma 1 and Theorems 1–3, a protocol-based FTKF mechanism is formalized to settle the federated filtering fusion problem in the presence of the dead-zone-like censoring, dynamical bias and RRP. The investigated model (1)–(8) is generic for its inclusion of not only the multi-sensor sampling nature, but also the modeling and observation uncertainties ( i.e. the dynamical bias and dead-zone-like censoring) which are universally confronted in engineering ranges such as image processing, target tracking, fault diagnosis, etc. These uncertainties are propitiously tackled in a holistic yet efficient framework under the RRP. It is noteworthy

TABLE I: FTKF Pseudocode

**Algorithm:** FTKF
**Input:** $\bar{x}_0$, $b_0$, $P_{\bar{x}_0}$,$P_{\bar{b}_0}$, $y_{m,1:k}$
**Output:** $\hat{x}_k$, $\hat{b}_k$, $P_{\tilde{x}_k}$.
1: let $\hat{\xi}_0 = \begin{bmatrix} \bar{x}_0^T & \bar{b}_0^T \end{bmatrix}^T$, $\hat{\xi}_{m,0} = \bar{\xi}_0$, $P_{\tilde{\xi}_{m,0}} = \epsilon_m^{-1} P_{\tilde{\xi}_0}$, $Q_{m,0} = \epsilon_m^{-1} Q_0$, $P_{\tilde{\xi}_0} = \text{diag}\{P_{\tilde{x}_0}, P_{\tilde{b}_0}\}$.
2: **for** $k = 1 : N$ **do**
3: calculate the local predicted estimate $\hat{\xi}^-_{m,k}$ and covariance $P_{\tilde{\xi}^-_{m,k}}$ by (18)–(19);,
4: calculate the local gain matrix $K_{m,k}$ by (22);
5: calculate the local updated estimate $\hat{\xi}_{m,k}$ and covariance $P_{\tilde{\xi}_{m,k}}$ by (20)–(21);
6: calculate the optimal fused estimate $\hat{\xi}_k$ and covariance $P_{\tilde{\xi}_k}$ by (26);
7 calculate the optimal fused estimates $\hat{x}_k$ and $\hat{b}_k$ and associate covariances $P_{\tilde{x}_k}$ and $P_{\tilde{b}_k}$ by (28)
8: reallocate $\hat{\xi}_{m,k}, P_{\tilde{\xi}_{m,k}}$ and $Q_{m,k}$ by (27);
9: **end for**

that the desired FTKF is, in essence, a distributed extension of the conventional TKF. In the event that the dynamical bias and the RRP are disregarded (i.e. $B_k = 0$ and $\bar{y}_{m,k} = z_{m,k}$), the LTKF in Theorem 1 will degrade to the standard TKF in [2]. Consequently, the FTKF in Theorem 2 will degenerate to the distributed generalization of the conventional TKF.

Next, we move forward to assess the performance of the designed FTKF. Due to the time-varying nature of the protocol-induced measurement update coefficient $\Gamma_{m,\hbar_k}$, the convergence of the developed federated Tobit Kalman filtering algorithm cannot be guaranteed in general. Thus, we turn to pursue the boundedness of the developed algorithm where the upper and lower bounds of the estimation error covariance are explored. The pursuit of such bounds can be carried out based on three principles: 1) the optimality of the developed LTKF motivates us to construct a set of suboptimal filters whose estimation error covariances are envisioned to be the upper bounds on $P_{\tilde{\xi}^-_{m,k}}$; 2) the semi-positive definiteness of $P_{\tilde{\xi}^-_{m,k}}$, $Q_k$ and $R_{m,k}$ paves the way for us to envisage the lower bound on $P_{\tilde{\xi}^-_{m,k}}$ via some subtle matrix manipulations; and 3) the federated fusion rule provides us with the correlation between the bounds of the LTKF and that of the fused filter.

Recalling that the optimal protocol-based LTKF derived in Theorem 2 has an optimal filtering gain $K_{m,k}$ (which depends on both left- and right-censoring probabilities $\bar{\alpha}_{m,k}$ and $\bar{\beta}_{m,k}$), the following theorem is dedicated to the derivation of a self-propagating upper bound on $P_{\tilde{\xi}^-_{m,k}}$ via constructing suboptimal protocol-based LTKFs with suboptimal filtering gains $K^u_{m,k}$ (which depends only on the left-censoring probabilities $\bar{\alpha}_{m,k}$). As to the lower bound on $P_{\tilde{\xi}_{m,k}}$, it can be acquired by making use of the semi-positive definiteness of matrices $P_{\tilde{\xi}^-_{m,k}}$, $Q_k$ and $R_{m,k}$.

*Theorem 4:* Let the initial condition $P^u_{\tilde{\xi}^-_{m,0}} > 0$ and $P^l_{\tilde{\xi}^-_{m,0}} > 0$ be given. Calculate the matrix sequences $\left\{ P^u_{\tilde{\xi}^-_{m,k+1}} \right\}_{k\geq 0}$ and $\left\{ P^l_{\tilde{\xi}^-_{m,k+1}} \right\}_{k\geq 0}$ according to the following difference

equations:

$$
\begin{aligned}
&P^{u}_{\tilde{\xi}^{-}_{m,k+1}} \\
=&\mathcal{A}_k P^{u}_{\tilde{\xi}^{-}_{k}} \mathcal{A}_k^T + \mathcal{B}_k Q_k \mathcal{B}_k^T - \mathcal{A}_k (1-\bar{\alpha}_{m,k})^2 P_{\tilde{\xi}^{-}_{m,k}} \\
&\times (\Gamma_{m,\hbar_k} C_{m,k})^T \Big\{ (1-\bar{\alpha}_{m,k})^2 \Gamma_{m,\hbar_k} C_{m,k} P_{\tilde{\xi}^{-}_{m,k}} C_{m,k}^T \Gamma_{m,\hbar_k}^T \\
&+ (1-\bar{\alpha}_{m,k})^2 \sum_{l=1}^{p-1} \Gamma_{m,\hbar_{k-l}} C_{m,k-l} P_{\tilde{\xi}^{-}_{m,k-l}} C_{m,k-l}^T \Gamma_{m,\hbar_{k-l}}^T \\
&+ \mathcal{R}_{m,k} \left[1+\varphi(\bar{\vartheta}^l_{m,k})\right] \Big\}^{-1} \Gamma_{m,\hbar_k} C_{m,k} P_{\tilde{\xi}^{-}_{m,k}} \mathcal{A}_k^T, \\
&P^{l}_{\tilde{\xi}^{-}_{m,k+1}} \\
=&\left(1-(1-\bar{\alpha}_{m,k}-\bar{\beta}_{m,k})^2\right) \mathcal{A}_k P^{l}_{\tilde{\xi}^{-}_{m,k}} \mathcal{A}_k^T + \mathcal{B}_k Q_k \mathcal{B}_k^T.
\end{aligned}
$$

Then, the calculated matrices $P^{u}_{\tilde{\xi}^{-}_{m,k+1}}$ and $P^{l}_{\tilde{\xi}^{-}_{m,k+1}}$ satisfy

$$P^{l}_{\tilde{\xi}^{-}_{m,k+1}} \leq P_{\tilde{\xi}^{-}_{m,k+1}} \leq P^{u}_{\tilde{\xi}^{-}_{m,k+1}},$$

i.e. $P^{u}_{\tilde{\xi}^{-}_{m,k+1}}$ and $P^{l}_{\tilde{\xi}^{-}_{m,k+1}}$ are, respectively, the self-propagating upper and lower bounds on $P_{\tilde{\xi}^{-}_{m,k+1}}$, where $\varphi(\bar{\vartheta}^l_{m,k}) = \lambda(\bar{\vartheta}^l_{m,k})[\lambda(\bar{\vartheta}^l_{m,k}) - \bar{\vartheta}^l_{m,k}]$ and $\lambda(\bar{\vartheta}^l_{m,k}) = \phi(\bar{\vartheta}^l_{m,k})/[1-\Phi(\bar{\vartheta}^l_{m,k})]$.

*Proof:* See Appendix–C. ■

*Theorem 5:* Letting the initial condition $P^{u}_{\tilde{\xi}^{-}_{m,0}} > 0$ and $P^{l}_{\tilde{\xi}^{-}_{m,0}} > 0$ be given, we have

$$P^{l}_{\tilde{x}^{-}_{k+1}} \leq P_{\tilde{x}^{-}_{k+1}} \leq P^{u}_{\tilde{x}^{-}_{k+1}},$$

i.e. $P^{u}_{\tilde{x}^{-}_{k+1}}$ and $P^{l}_{\tilde{x}^{-}_{k+1}}$ are, respectively, the self-propagating upper and lower bounds on $P_{\tilde{x}^{-}_{k+1}}$, where

$$
\begin{aligned}
P^{u}_{\tilde{x}^{-}_{k+1}} =& \Gamma_1 \left[ \sum_{m=1}^{p} \left( P^{u}_{\tilde{\xi}_{m,k}} \right)^{-1} \right]^{-1} \Gamma_1^T, \\
P^{l}_{\tilde{x}^{-}_{k+1}} =& \Gamma_1 \left[ \sum_{m=1}^{p} \left( P^{l}_{\tilde{\xi}_{m,k}} \right)^{-1} \right]^{-1} \Gamma_1^T.
\end{aligned}
$$

*Proof:* Theorem 5 follows directly from Theorems 2–4. ■

*Remark 7:* It should be noted that although the main results in this paper are obtained based on scalar sensor observation models for simplicity, they can be directly generalized to the case of multi-dimensional observation models. This generalization would brings in changes that include 1) the transformation of the update coefficient from $\Gamma_{m,\hbar_k} \triangleq \delta(\hbar_k - m)$ (which is a scalar) to $\Gamma_{m,\hbar_k} \triangleq \delta(\hbar_k - m)I$ (which is now a matrix); and 2) the introduction of a few more Bernoulli random variables $\alpha^i_{m,k}$ $(i = 1, 2, \ldots, n_{z_m})$ and $\beta^i_{m,k}$ that are adopted to regulate the left- and right-censoring of $y^i_{m,k}$ (which is the $i$th entry of $y_{m,k}$). Fortunately, the observation model can still be written in a form similar to (8), and this makes it possible for us to easily extend our main results in this paper to the case of multi-dimensional sensor observations.

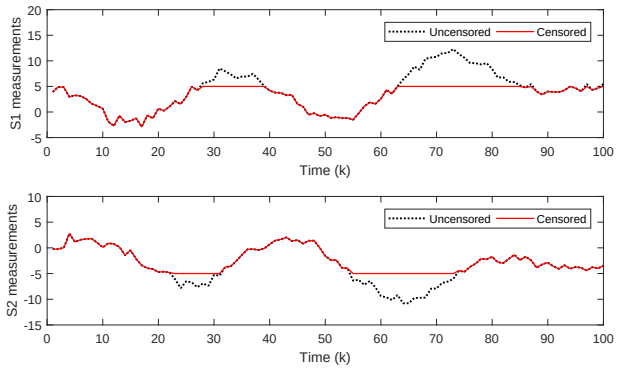


Fig. 2: $\bar{y}_{1,k}$, $\bar{y}_{2,k}$ (uncensored), and $y_{1,k}$ and $y_{2,k}$ (censored).

## IV. Illustrative Example

In this section, the oscillator example (modified from [1], [2])and distributed target tracking example are leveraged to elucidate the usefulness of the presented filter design approach and associated filtering performance. Denote the first and second dimensions of $x_k$, respectively, as $x_{1,k}$ and $x_{2,k}$, and the root mean-squared errors (RMSEs) and average root mean-squared errors (ARMSEs) of $x_{1,k}$, $x_{2,k}$ and $b_k$ as

$$
\begin{aligned}
\text{RMSE1} \triangleq& \sqrt{\frac{1}{M}\sum_{i=1}^{M}\left(x^{(i)}_{1,k} - \hat{x}^{(i)}_{1,k}\right)^2}, \\
\text{RMSE2} \triangleq& \sqrt{\frac{1}{M}\sum_{i=1}^{M}\left(x^{(i)}_{2,k} - \hat{x}^{(i)}_{2,k}\right)^2}, \\
\text{RMSE3} \triangleq& \sqrt{\frac{1}{M}\sum_{i=1}^{M}\left(b^{(i)}_{k} - \hat{b}^{(i)}_{k}\right)^2}, \\
\text{ARMSE1} \triangleq& \frac{1}{N}\sum_{k=1}^{N}\sqrt{\frac{1}{M}\sum_{i=1}^{M}\left(x^{(i)}_{1,k} - \hat{x}^{(i)}_{1,k}\right)^2}, \\
\text{ARMSE2} \triangleq& \frac{1}{N}\sum_{k=1}^{N}\sqrt{\frac{1}{M}\sum_{i=1}^{M}\left(x^{(i)}_{2,k} - \hat{x}^{(i)}_{2,k}\right)^2}, \\
\text{ARMSE3} \triangleq& \frac{1}{N}\sum_{k=1}^{N}\sqrt{\frac{1}{M}\sum_{i=1}^{M}\left(b^{(i)}_{k} - \hat{b}^{(i)}_{k}\right)^2},
\end{aligned}
$$

where $M$ is the number of Monte Carlo trials and $N$ is the number of time steps in each trial.

### A. Oscillator Example

Let system (1)-(8) have following parameters

$$
\begin{aligned}
A_k =& \begin{bmatrix} \cos(\omega) & -\sin(\omega) \\ \sin(\omega) & \cos(\omega) \end{bmatrix}, B_k = \begin{bmatrix} 0.1 \\ 0.15 \end{bmatrix}, \\
\Xi_k =& 0.25, C_{1,k} = \begin{bmatrix} 1 & 0 \end{bmatrix}, C_{2,k} = \begin{bmatrix} 0 & 1 \end{bmatrix}, \\
Q_k =& \text{diag}\{0.0025, 0.0025\}, R_{1,k} = R_{2,k} = 0.6, \\
H_k =& 1, \omega = 0.052\pi, \tau^l_1 = \tau^l_2 = -5, \tau^r_1 = \tau^r_2 = 5, \\
P_{\tilde{x}_0} =& 0.1 I_2, \bar{x}_0 = \begin{bmatrix} 5 & 0 \end{bmatrix}^T, \bar{b}_0 = 0, P_{\tilde{b}_0} = 0.1.
\end{aligned}
$$

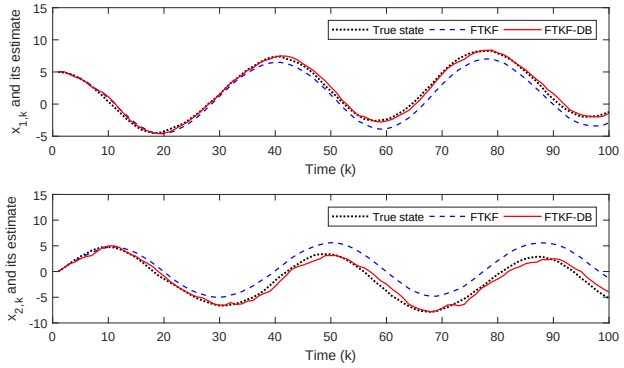


Fig. 3: States and Estimates.

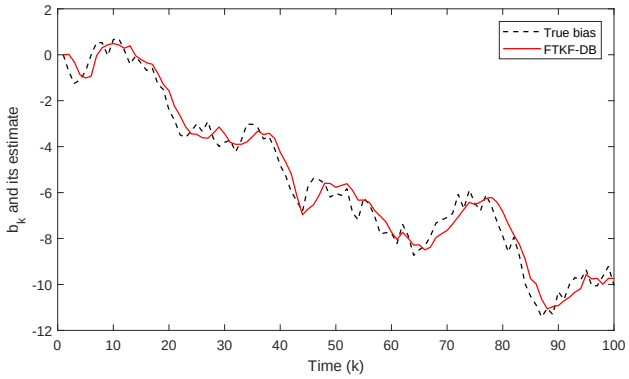


Fig. 4: The Bias and its estimate.

Note that the dynamic model is corrupted by ambient disturbances entering the system via the process noise $\omega_k$ and dynamical bias $b_k$. The magnetometer sampling is subject to the dead-zone-like censoring, and the data transmission is scheduled by the RRP. In the sequel, in order to testify the effectiveness of our filtering approach in appropriately addressing the dynamical bias issue, we first make a comparison between the proposed FTKF (which is barely capable of addressing the multi-sensor dead-zone-like censored observations in case of the RRP) and the FTKF with dynamical bias (FTKF-DB) (which is capable of simultaneously addressing the bias-corrupted dynamic model and the multi-sensor dead-zone-like censored observations in case of the RRP). From the following demonstrated figures, one can apparently observe the superiority of our FTKF-DB over the FTKF in accurately estimating the target state.

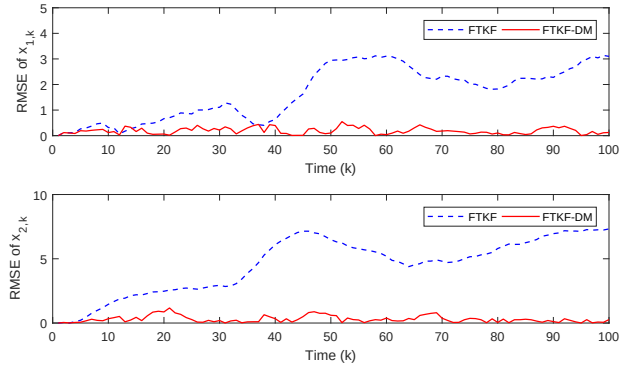


Fig. 5: Comparison in RMSE1 and RMSE2 between the FTKF and FTKF-DB.

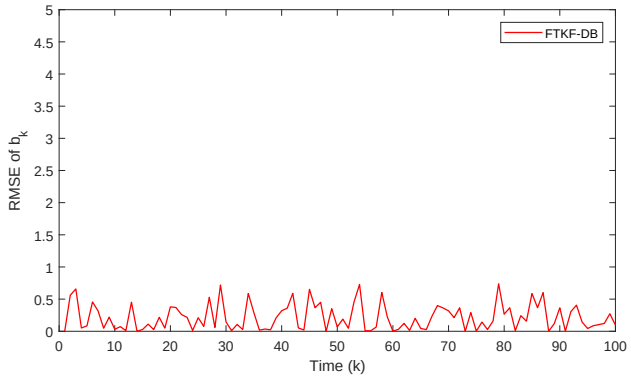


Fig. 6: RMSE3 produced by FTKF-DB.

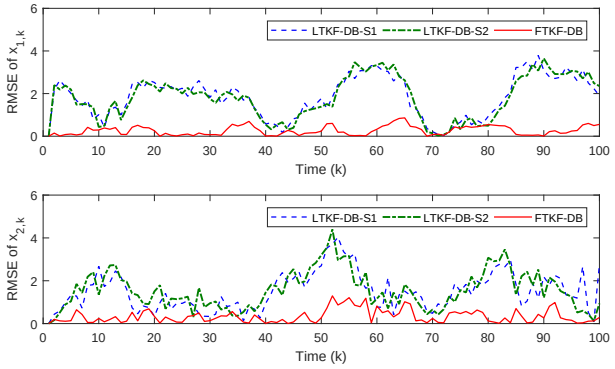


Fig. 7: Comparison in RMSE1 and RMSE2 between the local and fused filters.

For Sensor 1 (S1) and Sensor 2 (S2), Fig. 2 sketches the corresponding uncensored observations ($\bar{y}_{1,k}$ and $\bar{y}_{2,k}$) and censored observations ($y_{1,k}$ and $y_{2,k}$). Fig. 3 depicts the true state values and their estimates provided by the FTKF and FTKF-DB, and Fig. 4 illustrates the bias estimates produced by our FTKF-DB. It is seen from Figs. 3–4 that, our FTKF-DB manages to track the state and bias values precisely, whilst the FTKF has considerable deviations from true state values, and moreover, is unable to track the bias. Figs. 5–6 plot the RMSE curves of the FTKF and FTKF-DB after 1000 independent Mote Carlo trials. It is spotted from Figs. 5–6 that, the RMSE1 and RMSE2 curves of our FTKF-DB always reside lower than that of the FTKF, whilst the RMSE3 curve of our FTKF-DB is within a satisfactory range. This is because that both state and bias estimation issues are well settled in our FTKF-DB, whereas the bias estimation problem is not disposed of in the FTKF.

Besides, to further elaborate the superiority of our FTKF-

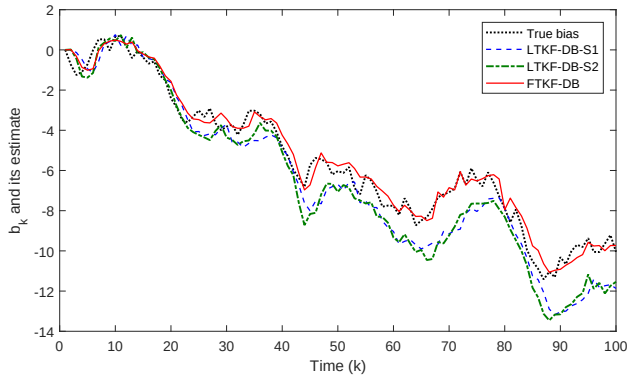


Fig. 8: Comparison in $\hat{b}_k$ between the local and fused filters.

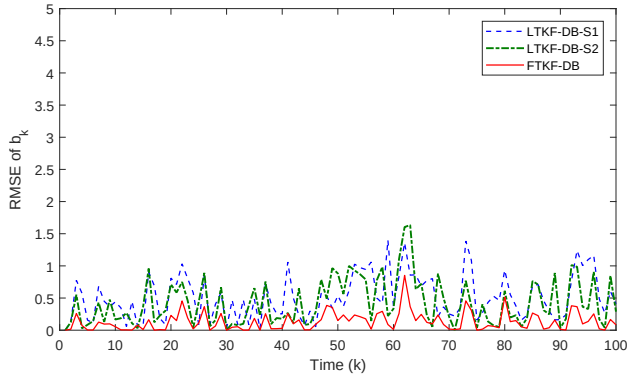


Fig. 9: Comparison in RMSE3 between the local and fused filters.

DB over its local counterparts, the performance comparison is made among these filters, where the LTKFs based on S1 and S2 observations are, respectively, named as LTKF-DB-S1 and LTKF-DB-S2. After 1000 times of Monte Carlo trials, Fig. 7 draws the RMSE curves in regard to the state tracking, whilst Figs. 8–9 demonstrate both estimation and RMSE curves with respect to the bias tracking. It is evidently seen from Figs. 7–9 that, the performance of our FTKF-DB outperforms that of the LTKF-DB-S1 and LTKF-DB-S2 in both state and bias tracking. This is because that our FTKF-DB properly integrates all available sensor information in accomplishing the task of target state and bias tracking, whilst both LTKF-DB-S1 and LTKF-DB-S2 produce their tracking results based at partial sensor observations.

TABLE II: Comparison among ARMSEs for different censoring regions $[\tau_m^l, \tau_m^r]$.

| $[\tau_m^l, \tau_m^r]$ | ARMSE1 | ARMSE2 | ARMSE3 |
|---|---|---|---|
| [-5, 5] | 0.2329 | 0.4768 | 0.2515 |
| [-1, 1] | 4.4252 | 4.1257 | 3.6580 |
| [-0.5, 0.5] | 7.1406 | 6.7888 | 5.7826 |

At last, we show the influences from the censoring threshold and noise covariance on the filtering algorithm of our FTKF-DB. For different censoring regions $[\tau_m^l, \tau_m^r]$ and noise covariances $R_{m,k}$, the associated ARMSEs of our developed filtering fusion algorithm based on 1000 Monte Carlo trials (with each trial comprised of 100 time steps) are demonstrated in Tables II–III. Looking at the two tables, we can draw the following conclusions: 1) as the censoring region $[\tau_m^l, \tau_m^r]$ narrows, the filtering accuracy with respect to the system state and dynamical bias deteriorates; and 2) as the covariance $R_{m,k}$ decreases, the filtering accuracy in regard to the system state and dynamical bias improves.

TABLE III: Comparison among ARMSEs for different noise covariances $R_{m,k}$.

| $R_{m,k}$ | ARMSE1 | ARMSE2 | ARMSE3 |
|---|---|---|---|
| 0.6 | 0.2329 | 0.4768 | 0.2515 |
| 0.1 | 0.0948 | 0.3707 | 0.2082 |
| 0.06 | 0.0742 | 0.2924 | 0.1601 |

### *B. Distributed Target Tracking Example*

Consider an example of distributive target tracking with two sensors. According to Newton's force principle, the movement of the target can be modeled as a constant-velocity nominal system and the target manoeuver is modeled as an unknown acceleration bias to the constant velocity. Meanwhile, the nominal system is corrupted by ambient disturbances entering the system via process noises. The two sensors sample the target position (range) and velocity (Doppler), respectively, with the same sampling period $T = 0.1s$. The measurement sampling is subject to the dead-zone-like censoring, and the data transmission is scheduled by the RRP. This situation can be modeled by (1)–(8) with following parameters.

$$
\begin{aligned}
&A_k = \begin{bmatrix} 1 & T \\ 0 & 1 \end{bmatrix}, B_k = \begin{bmatrix} 0.5T^2 \\ T \end{bmatrix}, \bar{x}_0 = \begin{bmatrix} 10 & 0 \end{bmatrix}^T, \bar{b}_0 = 0, \\
&\Xi_k = 0.25, C_{1,k} = \begin{bmatrix} 1 & 0 \end{bmatrix}, C_{2,k} = \begin{bmatrix} 0 & 1 \end{bmatrix}, P_{\tilde{x}_0} = I_2, \\
&H_k = 1, \tau_1^l = -1000, \tau_2^l = -200, \tau_1^r = 1000, \tau_2^r = 200, \\
&Q_k = 10^{-4}\text{diag}\{25, 25\}, R_{1,k} = 0.1, R_{2,k} = 0.3, P_{\tilde{b}_0} = 0.1.
\end{aligned}
$$

Figs. 10–11 plot the RMSE curves of the FTKF and FTKF-DB after 1000 independent Mote Carlo trials. It is spotted from Figs. 10–11 that, the RMSE curves with respect to the target position and velocity produced by our FTKF-DB always locate lower than that produced by the FTKF, whilst the RMSE curve in regard to the dynamical bias generated by our FTKF-DB is within a satisfactory range. These demonstration results obviously showcase the effectiveness and applicability of the proposed FTKF-DB in addressing the distributive target tracking problem subject to the dead-zone-like censoring, dynamical biases and RRP.

## V. Conclusion

In this paper, we have dealt with the filtering fusion problem for a class of multi-sensor systems with the concurrence of dead-zone-like censoring and dynamical biases under the RRP. The censoring phenomenon is depicted by the two-side Tobit

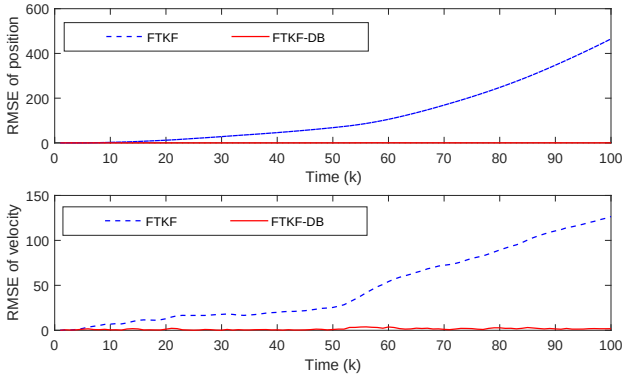


Fig. 10: Comparison in RMSEs of target position and velocity between the FTKF and FTKF-DB.

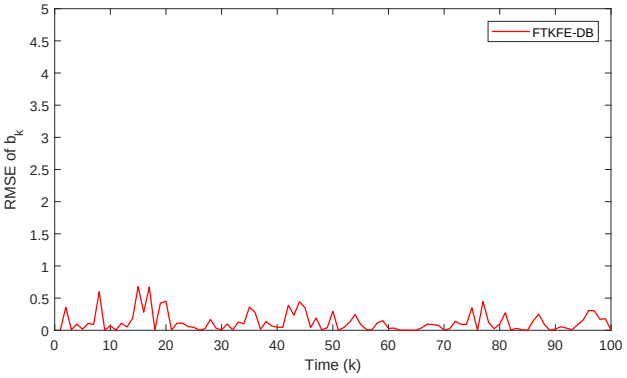


Fig. 11: RMSE of dynamical bias produced by FTKF-DB.

observation model to manifest the dead-zone-like feature of the observation. The bias takes the form of a dynamic model driven by Gaussian white noises with known means and variances. For each sensor, taking into consideration of the effects incurred by the censored observations, dynamic bias as well as RRP, an enhanced regression model has been constructed, based on which a unified filtering fusion framework has been formulated via the proposed LTKF. Thanks to the federated fusion rule, local estimates generated by all the LTKFs have been well incorporated to establish the desired FTKF. Finally, the applicability of the presented FTKF has been validated and its superiority over the local counterpart has also been certified by simulation experiments.

Further research topics would include the extension of our results to the more general systems with more complicated network-induced phenomena [10], [17], [27], [30]–[32], [35], [36], [43]. For instance,

- The multi-sensor Tobit Kalman filtering fusion problems with complicated network-induced phenomena, e.g. signal quantization, sensor saturation, and mixed time-delays.
- The multi-sensor Tobit Kalman filtering fusion problems for more general systems, e.g. sensor networks, complex networks and neural networks.

## APPENDIX

### A. Proof of Lemma 1

*Proof:* It is follows evidently from definitions

$$\begin{aligned}\bar{y}_{m,k} &\triangleq \zeta_{m,k} + \nu_{m,k},\\ \zeta_{m,k} &\triangleq \sum_{l=0}^{p-1} \Gamma_{m,\hbar_{k-l}} C_{m,k-l}\xi_{k-l},\\ \nu_{m,k} &\triangleq \sum_{l=0}^{p-1} \Gamma_{m,\hbar_{k-l}} \upsilon_{m,k-l}\end{aligned}$$

that $\nu_{m,k}$ is a zero mean Gaussian noise with covariance

$$\mathcal{R}_{m,k} \triangleq \sum_{l=0}^{p-1} \Gamma^2_{m,\hbar_{k-l}} R_{m,k-l}.$$

Accordingly, the PDF of $y_{m,k}$ has the following expression:

$$\begin{aligned}&f(y_{m,k}|x_k,\mathcal{R}_{m,k})\\ =&\frac{1}{\sqrt{\mathcal{R}_{m,k}}}\phi\left(\frac{y_{m,k}-\xi_{m,k}}{\sqrt{\mathcal{R}_{m,k}}}\right)u(y_{m,k}-\tau^l_m)\\ &\times u(\tau^r_m - y_{m,k})\\ &+\delta(y_{m,k}-\tau^l_m)\Phi(\vartheta^l_{m,k})+\delta(y_{m,k}-\tau^r_m)\\ &\times\left(1-\Phi(\vartheta^r_{m,k})\right),\end{aligned} \tag{29}$$

where $u(y_{m,k}-\tau^l_m)$ and $u(\tau^r_m - y_{m,k})$ are unit step functions, and $\phi\left(\frac{y_{m,k}-\xi_{m,k}}{\sqrt{\mathcal{R}_{m,k}}}\right)$ and $\Phi(\vartheta_{m,k})$ are calculated by (16)–(17).

In the light of (29), the mean of $y_{m,k}$ is

$$\begin{aligned}&\mathbb{E}\{y_{m,k}|x_{k,\mathcal{R}_{m,k}}\}\\ =&\text{Prob}\{\tau^l_m < y_{m,k} < \tau^r_m|x_k\}\\ &\times\mathbb{E}\{y_{m,k}|\tau^l_m < y_{m,k} < \tau^r_m, x_k\}\\ &+\text{Prob}\{y_{m,k}=\tau^l_m|x_k\}\mathbb{E}\{y_{m,k}|y_{m,k}=\tau^l_m,x_k\}\\ &+\text{Prob}\{y_{m,k}=\tau^r_m|x_k\}\mathbb{E}\{y_{m,k}|y_{m,k}=\tau^r_m,x_k\}\end{aligned} \tag{30}$$

To compute $\mathbb{E}\{y_{m,k}|x_k,\mathcal{R}_{m,k}\}$, the probabilities and expectations on the right-hand side of (30) must be provided.

$$\begin{aligned}&\text{Prob}\{\tau^l_m < y_{m,k} < \tau^r_m|x_k\}\\ =&\text{Prob}\{\tau^l_m < \bar{y}_{m,k} < \tau^r_m|x_k\}\\ =&\text{Prob}\{\tau^l_m - \zeta_{m,k} < \nu_{m,k} < \tau^r_m - \zeta_{m,k}|x_k\}\\ =&\Phi\left(\vartheta^r_{m,k}\right)-\Phi\left(\vartheta^l_{m,k}\right).\end{aligned} \tag{31}$$

In line with (29), we have

$$\begin{aligned}&\mathbb{E}\{y_{m,k}|\tau^l_m < y_{m,k} < \tau^r_m, x_k\}\\ =&\frac{1}{\sqrt{\mathcal{R}_{m,k}}}\int_{\tau^l_m}^{\tau^r_m} y_{m,k}\frac{\phi\left(\frac{y_{m,k}-\xi_{m,k}}{\sqrt{\mathcal{R}_{m,k}}}\right)}{\Phi\left(\vartheta^r_{m,k}\right)-\Phi\left(\vartheta^l_{m,k}\right)}d_{y_{m,k}}\\ =&\xi_{m,k}-\sqrt{\mathcal{R}_{m,k}}\lambda\left(\vartheta^r_{m,k},\vartheta^l_{m,k}\right),\end{aligned} \tag{32}$$

where $\lambda\left(\vartheta^r_{m,k},\vartheta^l_{m,k}\right)$ is computed by (14).

Parallel to (31)-(32), we attain

$$\text{Prob}\{y_{m,k}=\tau^l_m|x_k\}=\Phi\left(\vartheta^l_{m,k}\right), \tag{33}$$

$$\text{Prob}\{y_{m,k}=\tau^r_m|x_k\}=1-\Phi\left(\vartheta^r_{m,k}\right), \tag{34}$$

$$\mathbb{E}\{y_{m,k}|y_{m,k}=\tau_m^l,x_k\}=\tau_m^l, \tag{35}$$
$$\mathbb{E}\{y_{m,k}|y_{m,k}=\tau_m^r,x_k\}=\tau_m^r. \tag{36}$$

Inserting (31)-(36) into (30) yields

$$\begin{aligned}&\mathbb{E}\left\{y_{m,k}|x_k,\mathcal{R}_{m,k}\right\}\\=&\Phi\left(\vartheta_{m,k}^l\right)\tau_m^l+\left(1-\Phi\left(\vartheta_{m,k}^r\right)\right)\tau_m^r\\&+\left[\Phi\left(\vartheta_{m,k}^r\right)-\Phi\left(\vartheta_{m,k}^l\right)\right]\\&\times\left[\zeta_{m,k}-\sqrt{\mathcal{R}_{m,k}}\lambda\left(\vartheta_{m,k}^r,\vartheta_{m,k}^l\right)\right],\end{aligned}$$

which is precisely the same as (12).

Referring to (29), (32), (35) and (36) produces

$$\begin{aligned}&\text{var}\{y_{m,k}|y_{m,k}=\tau_m^l,x_k\}\\=&\text{var}\{y_{m,k}|y_{m,k}=\tau_m^r,x_k\}\\=&0,\end{aligned}$$

and therefore

$$\begin{aligned}&\text{var}\{y_{m,k}|x_k\}\\=&\text{var}\{y_{m,k}|\tau_m^l<y_{m,k}<\tau_m^r,x_k\}\\=&\mathbb{E}\{y_{m,k}^2|\tau_m^l<y_{m,k}<\tau_m^r,x_k\}\\&-\left(\mathbb{E}\{y_{m,k}^2|\tau_m^l<y_{m,k}<\tau_m^r,x_k\}\right)^2.\end{aligned} \tag{37}$$

The notice of (29) along with (32) tells

$$\begin{aligned}&\mathbb{E}\{y_{m,k}^2|\tau_m^l<y_{m,k}<\tau_m^r,x_k\}\\=&\frac{1}{\sqrt{\mathcal{R}_{m,k}}}\int_{\tau_m^l}^{\tau_m^r}y_{m,k}^2\frac{\phi\left(\frac{y_{m,k}-\xi_{m,k}}{\sqrt{\mathcal{R}_{m,k}}}\right)}{\Phi\left(\vartheta_{m,k}^r\right)-\Phi\left(\vartheta_{m,k}^l\right)}d_{y_{m,k}}\\=&\xi_{m,k}^2+\mathcal{R}_{m,k}-\sqrt{\mathcal{R}_{m,k}}\xi_{m,k}\lambda\left(\vartheta_{m,k}^r,\vartheta_{m,k}^l\right)\\&+\sqrt{\mathcal{R}_{m,k}}\frac{\left(\tau_m^l\phi\left(\vartheta_{m,k}^l\right)-\tau_m^r\phi\left(\vartheta_{m,k}^r\right)\right)}{\Phi\left(\vartheta_{m,k}^r\right)-\Phi\left(\vartheta_{m,k}^l\right)}.\end{aligned} \tag{38}$$

Inserting (32) and (38) into (37) gives

$$\text{var}\left\{y_{m,k}|x_k,\mathcal{R}_{m,k}\right\}=\mathcal{R}_{m,k}\left[1+\varphi\left(\vartheta_{m,k}^r,\vartheta_{m,k}^l\right)\right],$$

which is precisely the same as (13), where$\varphi\left(\vartheta_{m,k}^r,\vartheta_{m,k}^l\right)$ is provided by (15). ■

### B. Proof of Theorem 1

*Proof:* For the sake of derivation brevity, denote

$$P_{\xi_{m,k}\xi_{m,k-l}}\triangleq\mathbb{E}\{\xi_{m,k}\xi_{m,k-l}^T\},m=0,1\ldots,p-1,$$

and suppose

$$\begin{aligned}P_{\tilde{\xi}_k^-\tilde{\xi}_t^-}=&0\text{ for }k\neq t,k,t=1,2,\ldots,\\\text{cov}\{y_{m,k},y_{s,k}\}=&0\text{ for }m\neq s,m,s=1,2,\ldots,p.\end{aligned}$$

The extension to the setting where

$$\begin{aligned}P_{\tilde{\xi}_k^-\tilde{\xi}_t^-}\neq&0\text{ for }k\neq t,k,t=1,2,\ldots,\\\text{cov}\{y_{m,k},y_{s,k}\}\neq&0\text{ for }m\neq s,m,s=1,2,\ldots,p.\end{aligned}$$

is straightforward but rotationally cumbersome.

The orthogonality projection principle [4] tells us that, for system (10), its linear minimum variance estimate (based on the measurements from sensor $m$) is given by

$$\begin{aligned}\hat{\xi}_{m,k}=&\mathbb{E}\{\xi_k|y_{m,1:k}\}\\=&\mathbb{E}\{\xi_k|y_{m,1:k-1}\}+P_{\tilde{\xi}_{m,k}^-\tilde{y}_{m,k}^-}P_{\tilde{y}_{m,k}^-}^{-1}\\&\times\left(y_{m,k}-\mathbb{E}\{y_{m,k}|y_{m,1:k-1}\}\right)\\=&\hat{\xi}_{m,k}^-+K_{m,k}(y_{m,k}-\hat{y}_{m,k}^-),\end{aligned}$$

which is exactly the same as (20), where $K_{m,k}$ has the structure of (22). Meanwhile, we have

$$\begin{aligned}\hat{\xi}_{m,k}^-=&\mathbb{E}\{\xi_k|y_{m,1:k-1}\}\\=&\mathbb{E}\{\mathcal{A}_{k-1}\xi_{k-1}+\mathcal{B}_{k-1}w_{k-1}|y_{m,1:k-1}\}\\=&\mathbb{E}\{\mathcal{A}_{k-1}\xi_{k-1}|y_{m,1:k-1}\}\\=&\mathcal{A}_{k-1}\hat{\xi}_{m,k-1},\end{aligned}$$

which is exactly the same as (18), where the third equality holds from $\mathbb{E}\{w_{k-1}\}=0$.

Subtracting (18) from (10) brings

$$\tilde{\xi}_{m,k}^-=\mathcal{A}_{k-1}\tilde{\xi}_{m,k-1}^-+\mathcal{B}_{k-1}w_{k-1}.$$

Inserting the expression of $\tilde{\xi}_{m,k}^-$ into

$$P_{\tilde{\xi}_{m,k}^-}\triangleq\mathbb{E}\left\{\tilde{\xi}_{m,k}^-\left(\tilde{\xi}_{m,k}^-\right)^T\right\}$$

gives

$$\begin{aligned}P_{\tilde{\xi}_{m,k}^-}=&\mathbb{E}\Big\{\left(\mathcal{A}_{k-1}\tilde{\xi}_{m,k-1}^-+\mathcal{B}_{k-1}w_{k-1}\right)\\&\times\left(\mathcal{A}_{k-1}\tilde{\xi}_{m,k-1}^-+\mathcal{B}_{k-1}w_{k-1}\right)^T\Big\}\\=&\mathcal{A}_{k-1}P_{\tilde{\xi}_{m,k-1}^-}\mathcal{A}_{k-1}^T+\mathcal{B}_{k-1}Q_{k-1}\mathcal{B}_{k-1}^T,\end{aligned}$$

which is precisely the same as (19).

By resorting to Lemma 1, we have

$$\begin{aligned}\hat{y}_{m,k}^-=&\Phi\left(\bar{\vartheta}_{m,k}^l\right)\tau_m^l+\left(1-\Phi\left(\bar{\vartheta}_{m,k}^r\right)\right)\tau_m^r\\&+\left(\Phi\left(\bar{\vartheta}_{m,k}^r\right)-\Phi\left(\bar{\vartheta}_{m,k}^l\right)\right)\\&\times\left[\hat{\zeta}_{m,k}^-+\sqrt{\mathcal{R}_{m,k}}\lambda\left(\bar{\vartheta}_{m,k}^r-\bar{\vartheta}_{m,k}^l\right)\right]\\=&\bar{\alpha}_{m,k}\tau_m^l+\bar{\beta}_{m,k}\tau_m^r+(1-\bar{\alpha}_{m,k}-\bar{\beta}_{m,k})\\&\times\left[\hat{\zeta}_{m,k}^-+\sqrt{\mathcal{R}_{m,k}}\lambda\left(\bar{\vartheta}_{m,k}^r-\bar{\vartheta}_{m,k}^l\right)\right],\end{aligned}$$

which is precisely the same as (22).

Subtracting (22) from

$$\bar{y}_{m,k}\triangleq\zeta_{m,k}+\nu_{m,k}$$

leads to

$$\begin{aligned}\tilde{y}_{m,k}^-=&(1-\alpha_{m,k}-\beta_{m,k})\bar{y}_{m,k}+\alpha_{m,k}\tau_m^l\\&+\beta_{m,k}\tau_m^r-\hat{y}_{m,k}^-.\end{aligned} \tag{39}$$

Bearing (39) in mind, we have

$$\begin{aligned}&P_{\tilde{\xi}_{m,k}^-\tilde{y}_{m,k}^-}\\=&\mathbb{E}\Big\{\left(\xi_k-\hat{\xi}_k^-\right)\left((1-\alpha_{m,k}-\beta_{m,k})\bar{y}_{m,k}\right.\\&\left.+\alpha_{m,k}\tau_m^l+\beta_{m,k}\tau_m^r-\hat{y}_{m,k}^-\right)^T\Big\}\end{aligned}$$

$$
\begin{aligned}
=&\mathbb{E}\left\{(\xi_k(\zeta_{m,k}+\nu_{m,k})^T(1-\alpha_{m,k}-\beta_{m,k})\right\}\\
&-\mathbb{E}\left\{\hat{\xi}_k^-(\zeta_{m,k}+\nu_{m,k})^T(1-\alpha_{m,k}-\beta_{m,k})\right\}\\
=&\mathbb{E}\Bigg\{\xi_k\left(\sum_{l=0}^{p-1}\Gamma_{m,\hbar_{k-l}}C_{m,k-l}\xi_{k-l}\right)^T\\
&\times(1-\alpha_{m,k}-\beta_{m,k})\Bigg\}\\
&-\mathbb{E}\Bigg\{\hat{\xi}_k^-\left(\sum_{l=0}^{p-1}\Gamma_{m,\hbar_{k-l}}C_{m,k-l}\xi_{k-l}\right)^T\\
&\times(1-\alpha_{m,k}-\beta_{m,k})\Bigg\}\\
=&(1-\bar{\alpha}_{m,k}-\bar{\beta}_{m,k})\sum_{l=0}^{p-1}P_{\xi_{m,k}\xi_{m,k-l}}\\
&\times\left(\Gamma_{m,\hbar_{k-l}}C_{m,k-l}\right)^T-(1-\bar{\alpha}_{m,k}-\bar{\beta}_{m,k})\hat{\xi}_k^-\\
&\times\sum_{l=0}^{p-1}\hat{\xi}_{k-l}\left(\Gamma_{m,\hbar_{k-l}}C_{m,k-l}\right)^T. \qquad (40)
\end{aligned}
$$

Paying attention to the relationships among $\xi_{m,k}$, $\hat{\xi}_{m,k}$ and $\tilde{\xi}_{m,k}$, we have

$$
\begin{aligned}
P_{\xi_{m,k}\xi_{m,k-l}}=&\mathbb{E}\left\{\left(\tilde{\xi}_{m,k}^-+\hat{\xi}_{m,k}^-\right)\left(\tilde{\xi}_{m,k-l}^-+\hat{\xi}_{m,k-l}^-\right)^T\right\}\\
=&P_{\tilde{\xi}_{m,k}^-\tilde{\xi}_{m,k-l}^-}+\hat{\xi}_{m,k}^-\left(\hat{\xi}_{m,k-l}^-\right)^T, \qquad (41)
\end{aligned}
$$

where the second equality holds from

$$
\begin{aligned}
\mathbb{E}\left\{\tilde{\xi}_k^-\left(\hat{\xi}_{k-l}^-\right)^T\right\}=&0,\\
\mathbb{E}\left\{\hat{\xi}_k^-\left(\tilde{\xi}_{k-l}^-\right)^T\right\}=&0,
\end{aligned}
$$

Substituting (41) into (40) produces

$$
\begin{aligned}
P_{\tilde{\xi}_{m,k}^-\tilde{y}_{m,k}^-}=&(1-\bar{\alpha}_{m,k}-\bar{\beta}_{m,k})\sum_{l=0}^{p-1}P_{\tilde{\xi}_k^-\tilde{\xi}_{k-l}^-}\\
&\times\left(\Gamma_{m,\hbar_{k-l}}C_{m,k-l}\right)^T\\
=&(1-\bar{\alpha}_{m,k}-\bar{\beta}_{m,k})P_{\tilde{\xi}_k^-}\left(\Gamma_{m,\hbar_k}C_{m,k}\right)^T, \qquad (42)
\end{aligned}
$$

where the last equality holds from

$$P_{\tilde{\xi}_k^-\tilde{\xi}_t^-}\neq 0 \text{ for } k\neq t,\ k,t=0,1,2,\ldots.$$

(42) is precisely the same as (22).

Retrospecting the expressions of $\zeta_{m,k}$, $\hat{\zeta}_{m,k}^-$ and $\tilde{\zeta}_{m,k}^-$ leads to

$$
\begin{aligned}
\tilde{\zeta}_{m,k}^-=&\sum_{l=0}^{p-1}\Gamma_{m,\hbar_{k-l}}C_{m,k-l}\xi_{k-l}\\
&-\Gamma_{m,\hbar_k}C_{m,k}\hat{\xi}_k^--\sum_{l=1}^{p-1}\Gamma_{m,\hbar_{k-l}}C_{m,k-l}\hat{\xi}_{k-l}\\
=&\Gamma_{m,\hbar_k}C_{m,k}\tilde{\xi}_k^-+\sum_{l=1}^{p-1}\Gamma_{m,\hbar_{k-l}}C_{m,k-l}\tilde{\xi}_{k-l},
\end{aligned}
$$

which indicates

$$
\begin{aligned}
&\mathbb{E}\left\{\tilde{\zeta}_{m,k}^-\left(\tilde{\zeta}_{m,k}^-\right)^T\right\}\\
=&\Gamma_{m,\hbar_k}C_{m,k}P_{\tilde{\xi}_k^-}C_{m,k}^T\Gamma_{m,\hbar_k}\\
&+\sum_{l=1}^{p-1}\Gamma_{m,\hbar_{k-l}}C_{m,k-l}P_{\tilde{\xi}_{k-l}}C_{m,k-l}^T\Gamma_{m,\hbar_{k-l}}. \qquad (43)
\end{aligned}
$$

Akin to the derivation of $P_{\tilde{\xi}_{m,k}^-\tilde{y}_{m,k}^-}$, one has

$$
\begin{aligned}
P_{\tilde{y}_{m,k}^-}=&\mathbb{E}\left\{\tilde{y}_{m,k}^-\left(\tilde{y}_{m,k}^-\right)^T\right\}\\
=&(1-\bar{\alpha}_{m,k}-\bar{\beta}_{m,k})^2\mathbb{E}\left\{\tilde{\zeta}_{m,k}^-\left(\tilde{\zeta}_{m,k}^-\right)^T\right\}\\
&+\mathbb{E}\Big\{(1-\alpha_{m,k}-\beta_{m,k})\tilde{\nu}_{m,k}\tilde{\nu}_{m,k}^T\\
&\times(1-\alpha_{m,k}-\beta_{m,k})\Big\}, \qquad (44)
\end{aligned}
$$

where

$$\tilde{\nu}_{m,k}\triangleq\nu_{m,k}-\sqrt{\mathcal{R}_{m,k}}\lambda\left(\bar{\vartheta}_{m,k}^r-\bar{\vartheta}_{m,k}^l\right).$$

Accordingly, we have

$$
\begin{aligned}
&\mathbb{E}\Big\{(1-\alpha_{m,k}-\beta_{m,k})\tilde{\nu}_{m,k}\tilde{\nu}_{m,k}^T(1-\alpha_{m,k}-\beta_{m,k})\Big\}\\
=&\text{var}\left\{y_{m,k}|x_k,\mathcal{R}_{m,k},y_{m,1:k-1}\right\}\\
=&\mathcal{R}_{m,k}\left[1+\varphi\left(\bar{\vartheta}_{m,k}^r,\bar{\vartheta}_{m,k}^l\right)\right]. \qquad (45)
\end{aligned}
$$

Inserting (43) and (45) into (44) results in

$$
\begin{aligned}
&P_{\tilde{y}_{m,k}^-}\\
=&\mathbb{E}\left\{\tilde{y}_{m,k}^-\left(\tilde{y}_{m,k}^-\right)^T\right\}\\
=&(1-\bar{\alpha}_{m,k}-\bar{\beta}_{m,k})^2\Gamma_{m,\hbar_k}C_{m,k}P_{\tilde{\xi}_k^-}C_{m,k}^T\Gamma_{m,\hbar_k}\\
&+(1-\bar{\alpha}_{m,k}-\bar{\beta}_{m,k})^2\sum_{l=1}^{p-1}\Gamma_{m,\hbar_{k-l}}C_{m,k-l}P_{\tilde{\xi}_{k-l}}\\
&\times C_{m,k-l}^T\Gamma_{m,\hbar_{k-l}}+\mathcal{R}_{m,k}\left[1+\varphi\left(\bar{\vartheta}_{m,k}^r,\bar{\vartheta}_{m,k}^l\right)\right].l
\end{aligned}
$$

which is precisely the same as (23). ■

### C. Proof of Theorem 4

*Proof:* First, let us concentrate on designing a suboptimal protocol-based LTKF whose gain matrix $K_{m,k}^u$ only hinges on the left-censoring probability $\bar{\alpha}_{m,k}$. Recalling the LTKF designed in Theorem 2, its error covariance $P_{\tilde{\xi}_{m,k+1}^-}$ in (19) is rearranged into

$$
\begin{aligned}
&P_{\tilde{\xi}_{m,k+1}^-}\\
=&\mathcal{A}_kP_{\tilde{\xi}_{m,k}^-}\mathcal{A}_k^T+\mathcal{B}_kQ_k\mathcal{B}_k^T-(1-\bar{\alpha}_{m,k}-\bar{\beta}_{m,k})^2\mathcal{A}_kP_{\tilde{\xi}_{m,k}^-}\\
&\times\left(\Gamma_{m,\hbar_k}C_{m,k}\right)^T\Big\{(1-\bar{\alpha}_{m,k}-\bar{\beta}_{m,k})^2\Gamma_{m,\hbar_k}C_{m,k}P_{\tilde{\xi}_{m,k}^-}\\
&\times C_{m,k}^T\Gamma_{m,\hbar_k}^T+(1-\bar{\alpha}_{m,k}-\bar{\beta}_{m,k})^2\sum_{l=1}^{p-1}\Gamma_{m,\hbar_{k-l}}C_{m,k-l}\\
&\times P_{\tilde{\xi}_{m,k-l}^-}C_{m,k-l}^T\Gamma_{m,\hbar_{k-l}}^T
\end{aligned}
$$

$$+\mathcal{R}_{m,k}\left[1+\varphi(\bar{\vartheta}^r_{m,k},\bar{\vartheta}^l_{m,k})\right]\Big\}^{-1}\Gamma_{m,\hbar_k}C_{m,k}P_{\tilde{\xi}^-_{m,k}}\mathcal{A}_k^T. \tag{46}$$

Accordingly, the error covariance $P^u_{\tilde{\xi}^-_{m,k+1}}$ with regard to the suboptimal LTKF can be easily obtained as the one in Theorem 4

For $k=0$, by setting $P^u_{\tilde{\xi}^-_{m,0}}=P_{\tilde{\xi}^-_{m,0}}>0$, we easily have $P_{\tilde{\xi}^-_{m,0}}\leq P^u_{\tilde{\xi}^-_{m,0}}$. For $k>0$, since the performance of the optimal protocol-based LTKF must be no less than any of its suboptimal counterparts, it can be concluded that $P_{\tilde{\xi}^-_{m,k}}\leq P^u_{\tilde{\xi}^-_{m,k}}$. As such, $P^u_{\tilde{\xi}^-_{m,k}}$ in Theorem 4 is an upper bound on $P_{\tilde{\xi}^-_{m,k}}$ for all $k\geq 0$.

Next, we move forward to seek a lower bound on $P_{\tilde{\xi}^-_{m,k}}$. Denoting $\mathfrak{A}_{m,k}\triangleq\mathcal{A}_k+(1-\bar{\alpha}_{m,k}-\bar{\beta}_{m,k})^2\mathfrak{K}_{m,k}\Gamma_{m,\hbar_k}C_{m,k}$ and $\mathfrak{K}_{m,k}\triangleq-\mathcal{A}_{m,k}K_{m,k}$, we have

$$\begin{aligned}
&\mathfrak{A}_{m,k}P_{\tilde{\xi}^-_{m,k}}\left(\Gamma_{m,\hbar_k}C_{m,k}\right)^T+\mathfrak{K}_{m,k}\Big\{(1-\bar{\alpha}_{m,k}-\bar{\beta}_{m,k})^2\\
&\times\sum_{l=1}^{p-1}\Gamma_{m,\hbar_{k-l}}C_{m,k-l}P_{\tilde{\xi}^-_{m,k-l}}C^T_{m,k-l}\Gamma^T_{m,\hbar_{k-l}}\\
&+\mathcal{R}_{m,k}\left[1+\varphi(\bar{\vartheta}^r_{m,k},\bar{\vartheta}^l_{m,k})\right]\Big\}\\
=&\left(\mathcal{A}_k+(1-\bar{\alpha}_{m,k}-\bar{\beta}_{m,k})^2\mathfrak{K}_{m,k}\Gamma_{m,\hbar_k}C_{m,k}\right)P_{\tilde{\xi}^-_{m,k}}\\
&\times\left(\Gamma_{m,\hbar_k}C_{m,k}\right)^T+\mathfrak{K}_{m,k}\Big\{(1-\bar{\alpha}_{m,k}-\bar{\beta}_{m,k})^2\\
&\times\sum_{l=1}^{p-1}\Gamma_{m,\hbar_{k-l}}C_{m,k-l}P_{\tilde{\xi}^-_{m,k-l}}C^T_{m,k-l}\Gamma^T_{m,\hbar_{k-l}}\\
&+\mathcal{R}_{m,k}\left[1+\varphi(\bar{\vartheta}^r_{m,k},\bar{\vartheta}^l_{m,k})\right]\Big\}\\
=&\mathcal{A}_kP_{\tilde{\xi}^-_{m,k}}\left(\Gamma_{m,\hbar_k}C_{m,k}\right)^T+\mathfrak{K}_{m,k}P_{\tilde{y}^-_{m,k}}\\
=&0.
\end{aligned}\tag{47}$$

It follows from (46) that

$$\begin{aligned}
&P_{\tilde{\xi}^-_{m,k+1}}\\
=&\left(1-(1-\bar{\alpha}_{m,k}-\bar{\beta}_{m,k})^2\right)\left(\mathcal{A}_kP_{\tilde{\xi}^-_{m,k}}\mathcal{A}_k^T+\mathcal{B}_kQ_k\mathcal{B}_k^T\right)\\
&+(1-\bar{\alpha}_{m,k}-\bar{\beta}_{m,k})^2(\mathcal{A}_kP_{\tilde{\xi}^-_{m,k}}\mathcal{A}_k^T+\mathcal{B}_kQ_k\mathcal{B}_k^T)\\
&-(1-\bar{\alpha}_{m,k}-\bar{\beta}_{m,k})^2\mathcal{A}_kP_{\tilde{\xi}^-_k}\left(\Gamma_{m,\hbar_k}C_{m,k}\right)^T\\
&\times P^{-1}_{\tilde{y}^-_{m,k}}\Gamma_{m,\hbar_k}C_{m,k}P_{\tilde{\xi}^-_k}\mathcal{A}_k^T\\
=&\left(1-(1-\bar{\alpha}_{m,k}-\bar{\beta}_{m,k})^2\right)\left(\mathcal{A}_kP_{\tilde{\xi}^-_{m,k}}\mathcal{A}_k^T+\mathcal{B}_kQ_k\mathcal{B}_k^T\right)\\
&+(1-\bar{\alpha}_{m,k}-\bar{\beta}_{m,k})^2(\mathcal{A}_kP_{\tilde{\xi}^-_{m,k}}\mathcal{A}_k^T+\mathcal{B}_kQ_k\mathcal{B}_k^T)\\
&+(1-\bar{\alpha}_{m,k}-\bar{\beta}_{m,k})^2\mathfrak{K}_{m,k}\Gamma_{m,\hbar_k}C_{m,k}P_{\tilde{\xi}^-_{m,k}}\mathcal{A}_k^T\\
=&\left(1-(1-\bar{\alpha}_{m,k}-\bar{\beta}_{m,k})^2\right)\left(\mathcal{A}_kP_{\tilde{\xi}^-_{m,k}}\mathcal{A}_k^T+\mathcal{B}_kQ_k\mathcal{B}_k^T\right)\\
&+(1-\bar{\alpha}_{m,k}-\bar{\beta}_{m,k})^2\left(\mathfrak{A}_{m,k}P_{\tilde{\xi}^-_{m,k}}\mathcal{A}_k^T+\mathcal{B}_kQ_k\mathcal{B}_k^T\right).
\end{aligned}\tag{48}$$

Inserting (47) into (48) generates

$$\begin{aligned}
&P_{\tilde{\xi}^-_{m,k+1}}\\
=&\left(1-(1-\bar{\alpha}_{m,k}-\bar{\beta}_{m,k})^2\right)\left(\mathcal{A}_kP_{\tilde{\xi}^-_{m,k}}\mathcal{A}_k^T+\mathcal{B}_kQ_k\mathcal{B}_k^T\right)\\
&+(1-\bar{\alpha}_{m,k}-\bar{\beta}_{m,k})^2\left(\mathfrak{A}_{m,k}P_{\tilde{\xi}^-_{m,k}}\mathfrak{A}_k^T+\mathcal{B}_kQ_k\mathcal{B}_k^T\right)\\
&+(1-\bar{\alpha}_{m,k}-\bar{\beta}_{m,k})^2\mathfrak{K}_{m,k}P_{\tilde{y}^-_{m,k}}\mathfrak{K}^T_{m,k}\\
\geq&\left(1-(1-\bar{\alpha}_{m,k}-\bar{\beta}_{m,k})^2\right)\mathcal{A}_kP_{\tilde{\xi}^-_{m,k}}\mathcal{A}_k^T\\
&+(1-\bar{\alpha}_{m,k}-\bar{\beta}_{m,k})^2\mathcal{B}_kQ_k\mathcal{B}_k^T.
\end{aligned}\tag{49}$$

Inspired by (49), let us define

$$\begin{aligned}
P^l_{\tilde{\xi}^-_{m,k+1}}\triangleq&\left(1-(1-\bar{\alpha}_{m,k}-\bar{\beta}_{m,k})^2\right)\mathcal{A}_kP^l_{\tilde{\xi}^-_{m,k}}\mathcal{A}_k^T\\
&+(1-\bar{\alpha}_{m,k}-\bar{\beta}_{m,k})^2\mathcal{B}_kQ_k\mathcal{B}_k^T,
\end{aligned}$$

which is initialized at $P^l_{\tilde{\xi}^-_{m,0}}=0$. Now, let us prove $P^l_{\tilde{\xi}^-_{m,k+1}}\leq P_{\tilde{\xi}^-_{m,k+1}}$ via mathematical induction. Noticeably, at the initial time $k=0$, we have $P^l_{\tilde{\xi}^-_{m,0}}=0\leq P_{\tilde{\xi}^-_{m,0}}$. Supposing that $P^l_{\tilde{\xi}^-_{m,k}}\leq P_{\tilde{\xi}^-_{m,k}}$ holds at time $k$, we have

$$\begin{aligned}
P^l_{\tilde{\xi}^-_{m,k+1}}=&\left(1-(1-\bar{\alpha}_{m,k}-\bar{\beta}_{m,k})^2\right)\mathcal{A}_kP^l_{\tilde{\xi}^-_{m,k}}\mathcal{A}_k^T\\
&+(1-\bar{\alpha}_{m,k}-\bar{\beta}_{m,k})^2\mathcal{B}_kQ_k\mathcal{B}_k^T\\
\leq&\left(1-(1-\bar{\alpha}_{m,k}-\bar{\beta}_{m,k})^2\right)\mathcal{A}_kP_{\tilde{\xi}^-_{m,k}}\mathcal{A}_k^T\\
&+(1-\bar{\alpha}_{m,k}-\bar{\beta}_{m,k})^2\mathcal{B}_kQ_k\mathcal{B}_k^T\\
\leq&P_{\tilde{\xi}^-_{m,k+1}},
\end{aligned}$$

where the last inequality holds from (49). As a result, it can be concluded that, $P^l_{\tilde{\xi}^-_{m,k+1}}\leq P_{\tilde{\xi}^-_{m,k+1}}$ holds for all $k\geq 0$, i.e. $P^l_{\tilde{\xi}^-_{m,k+1}}$ given by (30) is a lower bound on $P_{\tilde{\xi}^-_{m,k+1}}$. As such, we have $P^l_{\tilde{\xi}^-_{m,k+1}}\leq P_{\tilde{\xi}^-_{m,k+1}}\leq P^u_{\tilde{\xi}^-_{m,k+1}}$ for all $k\geq 0$. This completes the proof. ■

## REFERENCES


[1] B. Allik, C. Miller, M. J. Piovoso, and R. Zurakowski, The Tobit Kalman filter: an estimator for censored measurements, *IEEE Transactions on Control Systems Technology*, vol. 24, no. 1, pp. 365–371, 2016.

[2] B. Allik, C. Miller, M. J. Piovoso, and R. Zurakowski, Estimation of saturated data using the Tobit Kalman filter, in *Proceedings of the American Control Conference*, Portland, OR, USA, Jun. 2014, pp. 4151–4156.

[3] T. Amemiya, Regression analysis when the dependent variable is truncated normal, *Econometrica*, vol. 41, no. 6, pp. 997–1016, 1973.

[4] B. D. O. Anderson, and J. B. Moore, Optimal Filtering. Englewood Cliffs, NJ, USA: Prentice-Hall, 1979.

[5] A. Assa, and F. Janabi-Sharifi, A robust vision-based sensor fusion approach for real-time pose estimation, *IEEE Transactions on Cybernetics*, vol. 44, no. 2, pp. 217–227, 2014.

[6] N. Carlson, Federated square root filter for decentralized parallel processes, *IEEE Transactions on Aerospace and Electronic Systems*, vol. 25, no. 3, pp. 517–525, 1990.

[7] Y. Chen, Z. Wang, L. Wang and W. Sheng, Finite-horizon $H_\infty$ state estimation for stochastic coupled networks with random inner couplings using Round-Robin protocol, *IEEE Transactions on Cybernetics*, in press, DOI: 10.1109/TCYB.2020.3004288.

[8] Y. Chen, Z. Wang, L. Wang and W. Sheng, Mixed $H_2/H_\infty$ state estimation for discrete-time switched complex networks with random coupling strengths through redundant channels, *IEEE Transactions on Neural Networks and Learning Systems*, vol. 31, no. 10, pp. 4130-4142, Oct. 2020.

[9] J. Ching, J. L. Beck, and K. A. Porter, Bayesian state and parameter estimation of uncertain dynamical systems, *Probabilistic Engineering Mechanics*, vol. 21, no. 1, pp. 81–96, 2006.

[10] Y. Cui, Y. Liu, W. Zhang and F. E. Alsaadi, Sampled-based consensus for nonlinear multiagent systems with deception attacks: The decoupled method, *IEEE Transactions on Systems, Man, and Cybernetics-Systems*, in press, DOI: 10.1109/TSMC.2018.2876497.

[11] Z. Du, and X. Li, Strong tracking Tobit Kalman filter with model uncertainties, *International Journal of Control, Automation and Systems*, vol. 17, no. 2, pp. 345–355, 2019.

[12] H. Fang, R. A. de Callafon, and J. Cortés, Simultaneous input and state estimation for nonlinear systems with applications to flow field estimation, *Automatica*, vol. 49, no. 3, pp. 2805–2812, 2013.

[13] B. Friedland, Treatment of bias in recursive filtering, *IEEE Transactions on Automatic Control*, vol. AC-14, no. 4, pp. 359–367, 1969.

[14] H. Geng, Z. Wang, and Y. Cheng, Distributed federated Tobit Kalman filter fusion over a packet-delaying network: a probabilistic perspective, *IEEE Transactions on Signal Processing*, vol. 66, no. 17, pp. 4477–4489, 2018.

[15] S. Gillijns, and B. De Moor, Unbiased minimum-variance input and state estimation for linear discrete-time systems, *Automatica*, vol. 43, no. 1, pp. 111–116, 2007.

[16] R. Gravina, P. Alinia, H. Ghasemzadeh, and G. Fortino, Multi-sensor fusion in body sensor networks: state-of-the-art and research challenges, *Information Fusion*, vol. 35, pp. 68–80, 2017.

[17] N. Hou, Z. Wang, D. W. C. Ho and H. Dong, Robust partial-nodes-based state estimation for complex networks under deception attacks, *IEEE Transactions on Cybernetics*, vol. 50, no. 6, pp. 2793–2802, Jun. 2020.

[18] N. Hou, Z. Wang, D. W. C. Ho and H. Dong, Robust partial-nodes-based state estimation for complex networks under deception attacks, *IEEE Transactions on Neural Networks and Learning Systems*, vol. 31, no. 6, pp. 2793–2802, Jun. 2020.

[19] C. -S. Hsieh, Robust two-stage Kalman filters for systems with unknown inputs, *IEEE Transactions on Automatic Control*, vol. 45, no. 12, pp. 2374–2378, 2000.

[20] C. -S. Hsieh, and F. -C. Chen, Optimal solution of the two-stage Kalman estimator, *IEEE Transactions on Automatic Control*, vol. 44, no. 1, pp. 194–199, 1999.

[21] J. Hu, Z. Wang, G.-P. Liu, H. Zhang and R. Navaratne, A prediction-based approach to distributed filtering with missing measurements and communication delays through sensor networks, *IEEE Transactions on Systems, Man, and Cybernetics-Systems*, in press, DOI: 10.1109/TSMC.2020.2966977.

[22] J. Huang, and X. He, Detection of intermittent fault for discrete-time systems with output dead-zone: a variant Tobit Kalman filtering approach, *Journal of Control Science and Engineering*, vol. 2017, art. no. 7849841, 9 pages, 2017.

[23] M. B. Ignagni, Optimal and suboptimal separate-bias Kalman estimators for a stochastic bias, *IEEE Transactions on Automatic Control*, vol. 45, no. 3, pp. 547–551, 2000.

[24] B. Khaleghi, A. Khamis, F. O. Karray, and S. N. Razavi, Multisensor data fusion: a review of the state-of-the-art, *Information Fusion*, vol. 14, no. 1, pp. 28-44, 2013.

[25] Y. Kim, and S. Lee, Energy-efficient wireless hospital sensor networking for remote patient monitoring, *Information Sciences*, vol. 282, pp. 332–349, 2014.

[26] H. Li, and Y. Shi, Robust $H_\infty$ filtering for nonlinear stochastic systems with uncertainties and Markov delays, *Automatica*, vol. 48, no. 1, pp. 159–166, 2012.

[27] Q. Li, B. Shen, Z. Wang and W. Sheng, Recursive distributed filtering over sensor networks on Gilbert-Elliott channels: A dynamic event-triggered approach, *Automatica*, vol. 113, Art. no. 108681, Mar. 2020.

[28] Q. Liu, Z. Wang, X. He and D. H. Zhou, On Kalman-consensus filtering with random link failures over sensor networks, *IEEE Transactions on Automatic Control*, vol. 63, no. 8, pp. 2701–2708, 2018.

[29] Q. Liu and Z. Wang, Moving-horizon estimation for linear dynamic networks with binary encoding schemes, *IEEE Transactions on Automatic Control*, in press, DOI: 10.1109/TAC.2020.2996579.

[30] L. Ma, Z. Wang, Y. Liu and F. E. Alsaadi, Distributed filtering for nonlinear time-delay systems over sensor networks subject to multiplicative link noises and switching topology, *International Journal of Robust and Nonlinear Control*, vol. 29, no. 10, pp. 2941–2959, Jul. 2019.

[31] L. Ma, Z. Wang, Q.-L. Han and H. K. Lam, Envelope-constrained $H_\infty$ filtering for nonlinear systems with quantization effects: The finite horizon case, *Automatica*, vol. 93, pp. 527–534, Jul. 2018.

[32] J. Mao, D. Ding, G. Wei and H. Liu, Networked recursive filtering for time-delayed nonlinear stochastic systems with uniform quantisation under Round-Robin protocol, *International Journal of Systems Science*, vol. 50, no. 4, pp. 871-884, Mar. 2019.

[33] H. Moradkhani, S. Sorooshian, H. V. Gupta, and P. R. Houser, Dual state-parameter estimation of hydrological models using ensemble Kalman filter, *Advances in Water Resources*, vol. 28, no. 2, pp. 135–147, 2005.

[34] I. Petersen, and M. R. James, Performance analysis and controller synthesis for nonlinear systems with stochastic uncertainty constraints, *Automatica*, vol. 32, pp. 959–972, 1996.

[35] B. Shen, Z. Wang, D. Wang, J. Luo, H. Pu and Y. Peng, Finite-horizon filtering for a class of nonlinear time-delayed systems with an energy harvesting sensor, *Automatica*, vol. 100, no. 2, pp. 144–152, Feb. 2019.

[36] B. Shen, Z. Wang, D. Wang and Q. Li, State-saturated recursive filter design for stochastic time-varying nonlinear complex networks under deception attacks, *IEEE Transactions on Neural Networks and Learning Systems*, in press, DOI: 10.1109/TNNLS.2019.2946290.

[37] Y. Shen, Z. Wang, B. Shen, F. E. Alsaadi, F. E. Alsaadi, Fusion estimation for multi-rate linear repetitive processes under weighted try-once-discard protocol, *Information Fusion*, vol. 55, pp. 281–291, 2020.

[38] D. Spinello, and D. J. Stilwell, Nonlinear estimation with state-dependent Gaussian observation noise, *IEEE Transactions on Automatic Control*, vol. 55, no. 6, pp. 1358–1366, 2010.

[39] Z. Utkovski, T. Eftimov, and P. Popovski, Random access protocols with collision resolution in a noncoherent setting, *IEEE Wireless Communications Letters*, vol. 4, no. 4, pp. 445–448, 2015.

[40] X. Wan, Z. Wang, M. Wu and X. Liu, $H_\infty$ state estimation for discrete-time nonlinear singularly perturbed complex networks under the Round-Robin protocol, *IEEE Transactions on Neural Networks and Learning Systems*, vol. 30, no. 2, pp. 415–426, Feb. 2019.

[41] G. Wang, N. Li, and Y. Zhang, An event based multi-sensor fusion algorithm with deadzone like measurements, *Information Fusion*, vol. 42, pp. 111–118, 2018.

[42] F. Wang, Z. Wang, J. Liang, and X. Liu, Recursive state estimation for two-dimensional shift-varying systems with random parameter perturbation and dynamical bias, *Automatica*, vol. 112, art. no. 108658, 2020.

[43] Y. Wang, Z. Wang, L. Zou, and H. Dong, Multi-loop decentralized $H_\infty$ fuzzy PID-like control for discrete time-delayed fuzzy systems under dynamical event-triggered schemes, *IEEE Transactions on Cybernetics*, in press, DOI: 10.1109/TCYB.2020.3025251.

[44] G. A. Watson, and W. D. Blair, Interacting acceleration compensation algorithm for tracking maneuvering targets, *IEEE Transactions on Aerospace and Electronic Systems*, vol. 31, no. 3, pp. 1152–1159, 1995.

[45] Z. Xiong, J. Chen, R. Wang, J. Liu, A new dynamic vector formed information sharing algorithm in federated filter, *Aerospace Science and Technology* vol. 29, pp. 37–46, 2013.

[46] L. Xu, X. R. Li, and Z. Duan, Hybrid grid multiple-model estimation with application to maneuvering target tracking, *IEEE Transactions on Aerospace and Electronic Systems*, vol. 52, no. 1, pp. 122–136, 2016.

[47] L. Yan, X. Li, Y. Xia, and M. Fu, Optimal sequential and distributed fusion for state estimation in cross-correlated noise, *Automatica*, vol. 49, no. 12, pp. 3607–3612, 2013.

[48] W. Zhang, and L. Shi, Sequential fusion estimation for clustered sensor networks, *Automatica*, vol. 89, pp. 358–363, 2018.

[49] Y. Zheng, R. Niu, and P. K. Varshney, Sequential Bayesian estimation with censored data for multi-sensor systems, *IEEE Transactions on Signal Processing*, vol. 62, no. 10, pp. 2626–2641, 2014.

[50] L. Zou, Z. Wang, Q.-L. Han and D. H. Zhou, Moving horizon estimation of networked nonlinear systems with random access protocol, *IEEE Transactions on Systems, Man, and Cybernetics-Systems*, in press, DOI: 10.1109/TSMC.2019.2918002.

[51] L. Zou, Z. Wang, J. Hu, and D. Zhou, Moving horizon estimation with unknown inputs under dynamic quantization effects, *IEEE Transactions on Automatic Control*, vol. 65, no. 12, pp. 5368-5375, Dec. 2020.

[52] L. Zou, Z. Wang, and D. Zhou, Moving horizon estimation with non-uniform sampling under component-based dynamic event-triggered transmission, *Automatica*, vol. 120, Art. no. 109154, 13 pages, Oct. 2020.

[53] L. Zou, Z. Wang, Q.-L. Han and D. H. Zhou, Moving horizon estimation for networked time-delay systems under Round-Robin protocol, *IEEE Transactions on Automatic Control*, vol. 64, no. 12, pp. 5191–5198, Dec. 2019.

**Hang Geng** received the B.Sc. degree in electronic information engineering in 2011 from Civil Aviation Flight University of China, Guanghan, China, and the Ph.D. degree in control science and engineering in 2017 from Northwestern Polytechnical University, Xi'an, China.

He is currently an Associate Professor in the School of Automation Engineering, University of Electronic Science and Technology of China, Chengdu, China. From 2015 to 2016, he was a visiting Ph.D. student with the Department of Computer Science, Brunel University London, Uxbridge, U.K. From 2018 to 2019, he was a Post-Doctoral Fellow with the Department of Mechanical Engineering, University of Kansas, Lawrence, U.S. From 2019 to 2020, he was a Research Fellow with the Department of Computer Science, Brunel University London, Uxbridge, U.K. His research interests include information fusion, fault diagnosis and state estimation.

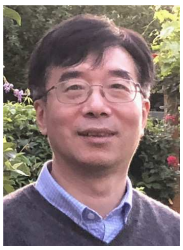

**Zidong Wang** (SM'03-F'14) was born in Jiangsu, China, in 1966. He received the B.Sc. degree in mathematics in 1986 from Suzhou University, Suzhou, China, and the M.Sc. degree in applied mathematics in 1990 and the Ph.D. degree in electrical engineering in 1994, both from Nanjing University of Science and Technology, Nanjing, China.

He is currently Professor of Dynamical Systems and Computing in the Department of Computer Science, Brunel University London, U.K. From 1990 to 2002, he held teaching and research appointments in universities in China, Germany and the UK. Prof. Wang's research interests include dynamical systems, signal processing, bioinformatics, control theory and applications. He has published 250+ papers in IEEE Transactions and 60+ papers in Automatica. He is a holder of the Alexander von Humboldt Research Fellowship of Germany, the JSPS Research Fellowship of Japan, William Mong Visiting Research Fellowship of Hong Kong.

Prof. Wang serves (or has served) as the Editor-in-Chief for *Neurocomputing*, the Deputy Editor-in-Chief for *International Journal of Systems Science*, and an Associate Editor for 12 international journals including IEEE Transactions on Automatic Control, IEEE Transactions on Control Systems Technology, IEEE Transactions on Neural Networks, IEEE Transactions on Signal Processing, and IEEE Transactions on Systems, Man, and Cybernetics-Part C. He is a Member of the Academia Europaea, a Fellow of the IEEE, a Fellow of the Royal Statistical Society and a member of program committee for many international conferences.

**Fuad E. Alsaadi** received the B.Sc. and M.Sc. degrees in electronic and communication from King AbdulAziz University, Jeddah, Saudi Arabia, in 1996 and 2002. He then received the Ph.D. degree in Optical Wireless Communication Systems in 2011 from the University of Leeds, Leeds, U.K.

Between 1996 and 2005, he worked in Jeddah as a communication instructor in the College of Electronics & Communication. He is currently an Associate Professor of the Electrical and Computer Engineering Department within the Faculty of Engineering, King Abdulaziz University, Jeddah, Saudi Arabia. He published widely in the top IEEE communications conferences and journals and has received the Carter award, University of Leeds for the best Ph.D. He has research interests in optical systems and networks, signal processing, synchronization and systems design.

**Khalid H. Alharbi** received the Ph.D. degree in electrical engineering in 2016 from the University of Glasgow, Glasgow, U.K.

He is currently an Assistant Professor in the Department of Electrical and Computer Engineering at King Abdulaziz University, Jeddah, Saudi Arabia. His research interest includes micro/nano-fabrication technologies, millimeter wave and THz antennas, and RTD-based devices.

**Yuhua Cheng** (M'11-SM'13) received the Ph.D. degree in instrumentation science and technology in 2007 from Sichuan University, Chengdu, China.

He is currently a Professor of Instrument Science and Technology in the School of Automation Engineering, University of Electronic Science and Technology of China, Chengdu, China. From 2013 to 2014, he was a Guest Researcher at the University of Toronto, Toronto, Canada. His research interests include electronic instrumentation, imaging/sensing for nondestructive evaluation, intelligent prognostics and health management of complex systems, and numerical modeling and simulation. Prof. Cheng is currently serving as an Associate Editor for Neurocomputing and IEEE Transactions on Instrumentation and Measurement, and a very active reviewer for many international journals.